Australian Seismological Reference Model (AuSREM): Mantle Component

B.L.N. Kennett[1], A. Fichtner[2], S. Fishwick[3] & K. Yoshizawa [4]

[1] *Research School of Earth Sciences, The Australian National University, Canberra ACT* 0200*, Australia*

[2] *Dept. of Earth Sciences, Utrecht University, Budapestlaan 4, 3584 CD, Utrecht, The Netherlands*

[3] *Dept. of Geology, University of Leicester, University Road, Leicester, LE1 7RH, UK*

[4] *Earth and Planetary Dynamics, Department of Natural History Sciences, Graduate School of Science, Hokkaido University, N10W8 Kita-ku, Sapporo 060810, Japan*

ABSTRACT

The mantle component of the Australian Seismological Reference Model (AuSREM) has been constructed from Australian specific sources, primarily exploiting the wealth of seismic sources at regional distances around Australia recorded at portable and permanent stations on the continent. AuSREM is designed to bring together the existing information on Australia, from both body wave and surface wave studies and provide a synthesis in the form of a 3-D model that can provide the basis for future refinement. The model is grid based with a 0.5° sampling in latitude and longitude, and is designed to be fully interpolable, so that properties can be extracted at any point.

For the upper mantle the primary source of information comes from seismic surface wave tomography, supplemented by analysis of body wave arrivals and regional tomography which provide useful constraints on the relation between P and S wavespeeds in the mantle lithosphere. A representative model has been developed to capture the features of mantle structure drawing on a range of studies. The mantle structure is represented by grid values at 25 km intervals in depth from 75–300 km. Shallower structure is linked to the AuSREM crust through the recent Moho depth model of Kennett et al. (2011), which exploits all available sources of seismological information. Below 300 km depth and in the surrounding area AuSREM is linked to the S40RTS model of Ritsema et al. (2011).

Key words: Australia, Mantle, Surface Waves, Tomography

1 INTRODUCTION

There have been a wide range of studies of the upper mantle beneath Australia exploiting the large amplitude surface waves and multiple S waves in the later parts of seismograms from events in the earthquake belts around Australia. These studies have exploited recordings at portable broad-band seismic stations and the limited number of high-quality permanent stations (see, e.g., Debayle & Kennett 2003). Now full continental coverage is available, the large scale features of wavespeed structure are well delineated, and agree well with results from body wave studies at much higher frequency.

The mantle component of the Australian Seismological Reference Model (AuSREM) is built from a suite of estimates of mantle structure based on different styles of analysis and inversion, and incorporates constraints from both surface and body-wave studies, as well as delay time tomography. The aim is to provide a representation of the 3-D structure in the mantle beneath Australia and its environs that captures the major features of the structure in a form that can be used in a range of applications, and provide a starting point for more detailed work.

A general description of the AuSREM project is given by Kennett & Salmon (2012), and a detailed discussion of the construction of the crustal component is to be found in Salmon et al. (2012). The first phase of the work was the generation of a new model for Moho depth exploiting the full range of relevant seismological information (Kennett et al. 2011), and this Moho distribution provides the link between the crustal and mantle components of AuSREM. The reference model is built on the full range of crustal and mantle studies using Australian specific information, the aim is to provide a model which captures the major features of lithospheric structure as revealed by both seismic body wave and surface wave studies, and hence is suitable for geodynamic interpretation. Potential applications of AuSREM include the delineation of major structural features and improved earthquake source characterisation, both within Australia and at the immediate plate boundaries by using better representations of crustal and mantle structure in source inversion and event location.

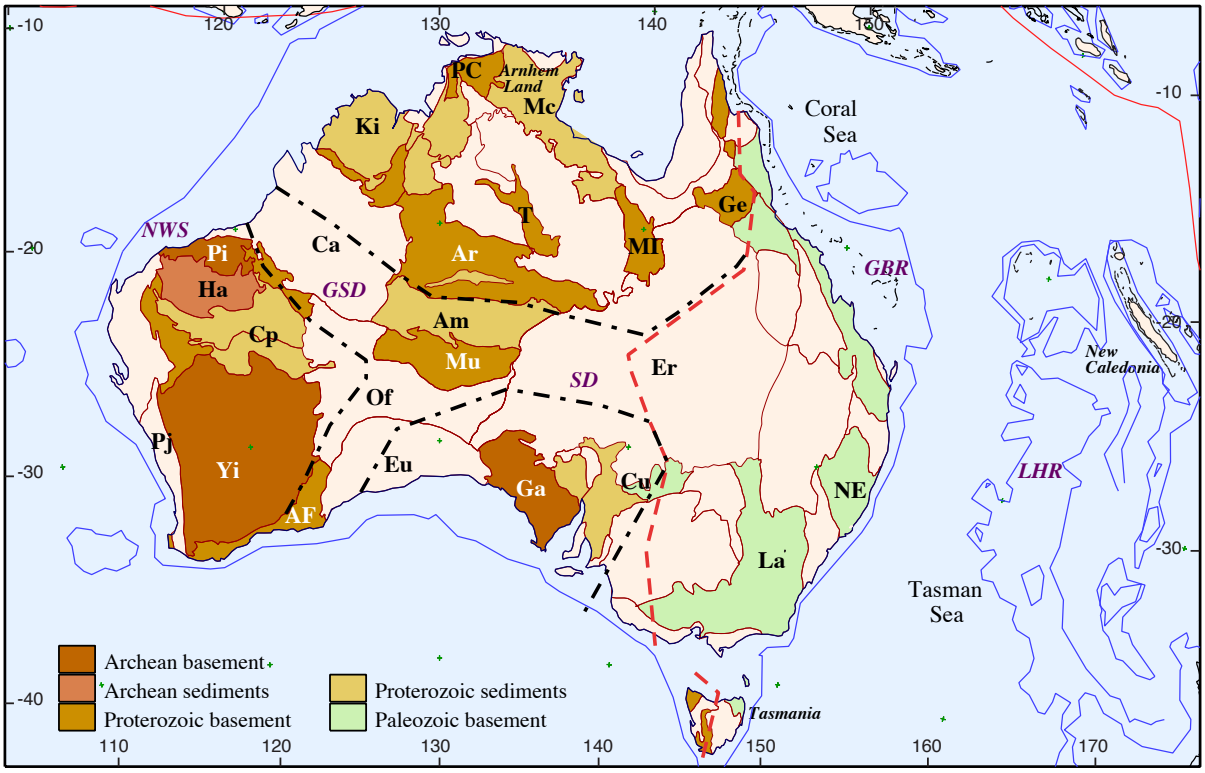

Figure 1. Simplified representation of the main tectonic features of Australia and its surroundings. The outline of the major cratons are marked by chain-dotted lines. The Tasman line in red is based on the reinterpretation by Direen & Crawford (2003). Key to marked features: AF - Albany-Fraser belt, Ar - Arunta Block, Am - Amadeus Basin, Ca - Canning Basin, Cp - Capricorn Orogen, Cu - Curnamona craton, Er - Eromanga Basin, Eu - Eucla Basin, Ga - Gawler craton, Ge - Georgetown inlier, Ha - Hamersley Basin, Ki - Kimberley Block, La - Lachlan Orogen, Mc - MacArthur Basin, MI - Mt Isa Block, Mu - Musgrave Block, NE - New England Orogen, Of - Officer Basin, PC - Pine Creek Inlier, Pi - Pilbara craton, Pj - Pinjarra Orogen, T - Tennant Creek Block, Yi - Yilgarn craton, *NWS* - Northwest Shelf, *GBR* - Great Barrier Reef, *LHR* - Lord Howe Rise, *SD* - Simpson Desert, *GSD* - Great Sandy Desert.

TECTONIC SETTING

The exposed geology of the Australian continent is composed of an assemblage of crustal blocks that can be broadly grouped into the Precambrian western and central cratonic zones and the Phanerozoic eastern province (Figure 1). Cratonic fusion was complete by around 1900 Ma, and the Precambrian core was left after the break up of Rodinia around 800 Ma. The east of Australia was an accretionary margin through the Palaeozoic with a sequence of subduction complexes on the margin of Gondwana progressively building to the east. Australia parted company with East Antarctica by around 80 Ma, and later the opening of the Tasman Sea from 80-60 Ma separated the Lord Howe Rise from eastern Australia to leave a submerged continental ribbon. Neogene volcanism along the eastern margin has left chains of volcanic edifices on land and in the Tasman sea, with eruptions as recent as 4000 BCE at Mt Gambier (38°S, 141°E).

The tectonic assemblage has left its imprint on the mantle. Thick lithosphere with high seismic wavespeed lies beneath the centre and west of the continent, and much thinner lithosphere is present in the east and into the Tasman Sea (see e.g. Fishwick et al. 2008).

2 DATA SOURCES

Major earthquake belts are associated with the subduction zones to the north and east of Australia from Indonesia to Vanuatu and the Tonga-Kermadec system, through New Zealand and into the Macquarie ridge. Less frequent seismicity occurs on the mid-ocean ridge between Australia and Antarctica. These earthquakes along the Australian plate margins provide events that lie at suitable distances from stations on the continent to be used as probes for upper mantle structure. The frequency of regional events is high, and so good coverage can be achieved in a few months. This has enabled campaigns of deployments of portable broad-band stations to supplement the limited number of high-fidelity permanent stations. The systematic use of portable stations was pioneered with the SKIPPY experiment (van der Hilst et al. 1994), where a group of stations were progressively moved across the continent in a sequence of deployments. Since 2005 number of new permanent stations have been installed by Geoscience Australia as part of an enhanced tsunami warming system, and these provide a useful supplement to the available data.

The combination of a long duration of recording at the permanent stations, and the broad spatial coverage from the portable stations provides an excellent resource for studies of the lithosphere. A wide range of techniques exploiting different aspects of seismograms, have

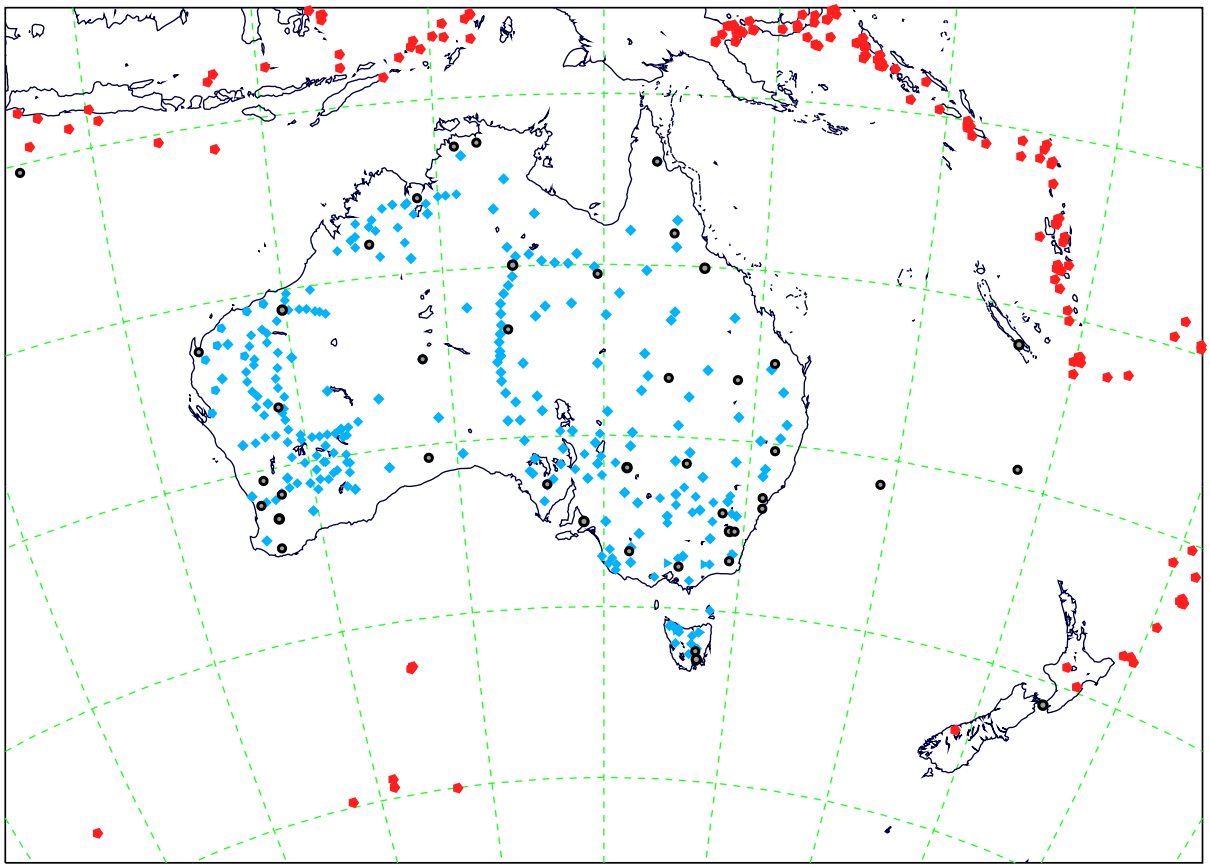

Figure 2. Configuration of seismic stations in Australia, permanent stations are shown in black and the portable broad-band stations in blue, together with seismic events with $M_s \geq 5$ for the year 2001, to illustrate the potential coverage.

been employed to extract information on the 3-D structure in the crust and mantle. These studies have used both the large amplitude surface wave components, but also higher frequency body waves in a variety of ways.

In addition to the broad-band studies, much denser deployments of shorter period stations have been made in southeastern Australia since 1999. These stations have mainly been employed in tomographic studies of the crust and uppermost mantle. Initially studies were made from the individual deployments, but the data from the whole sequence of station arrays has now been brought together in the WOMBAT project (Rawlinson et al. 2011).

The combination of the permanent and portable stations in Australia and its neighbours (Figure 2), with the wealth of regional earthquakes provides a configuration in which good sampling of the continent can be achieved. The absence of a regular supply of earthquakes to the west means that there is limited east-west control on the western margin of Australia. In contrast the area of the northern Tasman Sea on the eastern margin has excellent multi-directional coverage.

Prior studies

Much of what we know about the upper mantle structure under Australia has come from the exploitation of the multiply reflected shear waves and surface waves from regional earthquakes. These phases form the most prominent part of seismograms in the period range from 20 to 200 s. A variety of techniques have been employed to extract information on 3-D structure. One approach is to extract path-specific velocity models using either direct inversion of a portion of the seismogram (e.g., Simons et al. 2002), or secondary variables that improve the linearity of the inversion (e.g., Debayle & Kennett 2000; Fishwick et al. 2005). These path-based models can then be combined in a linear inversion for 3-D shear wavespeed structure. An alternative approach via the construction of phase speed maps for multiple modes and frequencies allows the incorporation of finite-frequency sampling (Yoshizawa & Kennett 2004). The most sophisticated approach is a fully nonlinear inversion of the waveforms using 3-D models from the outset (Fichtner et al. 2009, 2010). This computationally intensive approach has been based on the spectral element technique for modelling the wave propagation and adjoint methods to extract the necessary derivatives, which naturally include all finite-frequency effects.

The result of this range of different approaches is that structural variations have been imaged on scales down to 250 km horizontally and 30 km vertically. Significant substructure appears within the zones of both higher and lowered wavespeeds (Figures 3 and 4). The major features of all the recent models are concordant, and this provides the basis for constructing a representative model.

We also have information from studies of body waves at much higher frequencies from the same regional sources. Kaiho & Kennett

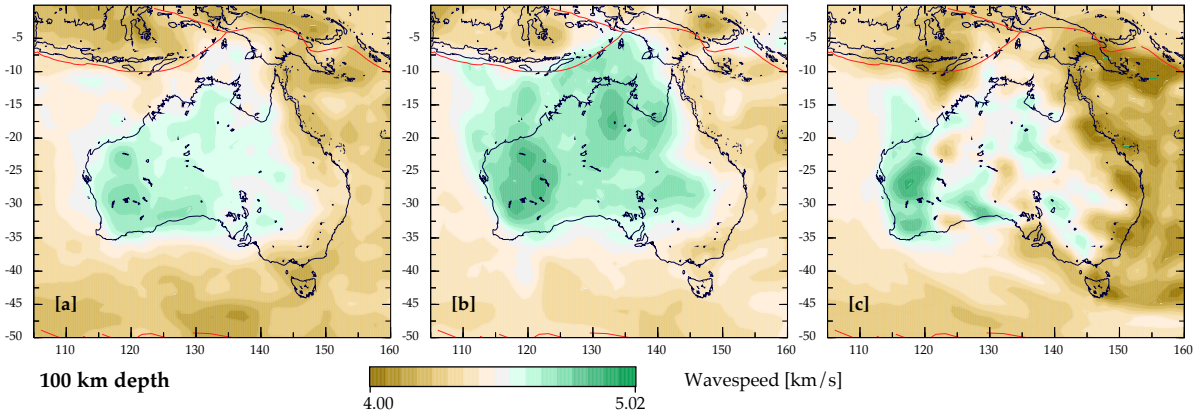

Figure 3. Shear wavespeed for the three base SV models at 100 km depth: (a) from Fishwick et al. (2008), (b) an update of the Yoshizawa & Kennett (2004) model, (c) from Fichtner et al. (2010) from full 3-D waveform inversion.

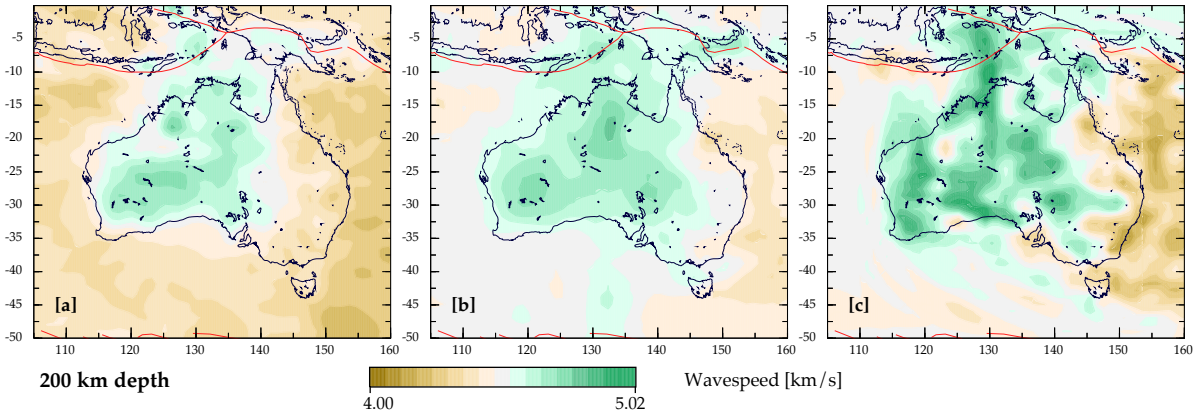

Figure 4. Shear wavespeed for the three base SV models at 200 km depth: (a) from Fishwick et al. (2008), (b) an update of the Yoshizawa & Kennett (2004) model, (c) from Fichtner et al. (2010) from full 3-D waveform inversion.

(2000) undertook a study of refracted waves through the upper mantle. They built record sections for a suite of corridors across the continent, and then used this information to extract 3-D structure under northern Australia for both P and S wavespeeds. This work provides valuable information on the relation between P and S wavespeeds and its likely geographical variation. Subsequently tomographic inversion for the refracted phases has been conducted for both P and S wavespeeds, in the context of studying the attenuation structure beneath the Australian region (Kennett & Abdulah 2011).

In addition we can make use of tomographic inversions carried out using principally teleseismic arrivals for both P and S waves (e.g., Gorbatov and Kennett, 2003). Such studies provide good horizontal resolution, but the limited range of angles of incidence means that there is a tendency for some smearing of structure in the vertical direction.

3 LITHOSPHERIC MODEL

There are two different approaches that can be employed to develop a reference model. The first is to use a specific inversion based on one style of information using as comprehensive a coverage as possible. For instance, Schivardi & Morelli (2011) inverted for mantle structure using group velocity information for the European region exploiting the improved crustal model developed by Molinari & Morelli (2011). In this way a model is secured that is firmly linked to a particular data set, but which may well not be as effective when used for other purposes. The second approach is to build on a compilation of structural information from a variety of sources to extract a model that includes elements from many different sources. This second style of model has been commonly used in crustal studies (e.g., Molinari & Morelli 2011, Salmon et al. 2013), and has the merit of building on all available sources of information. However, the resulting model may well not fit any specific data set as well as a model constructed for the purpose.

Rather than undertake a new inversion, we build on the information available from previous studies to build a representative model for the mantle component of AuSREM. The general consistency between the different models from surface wave studies and the results from

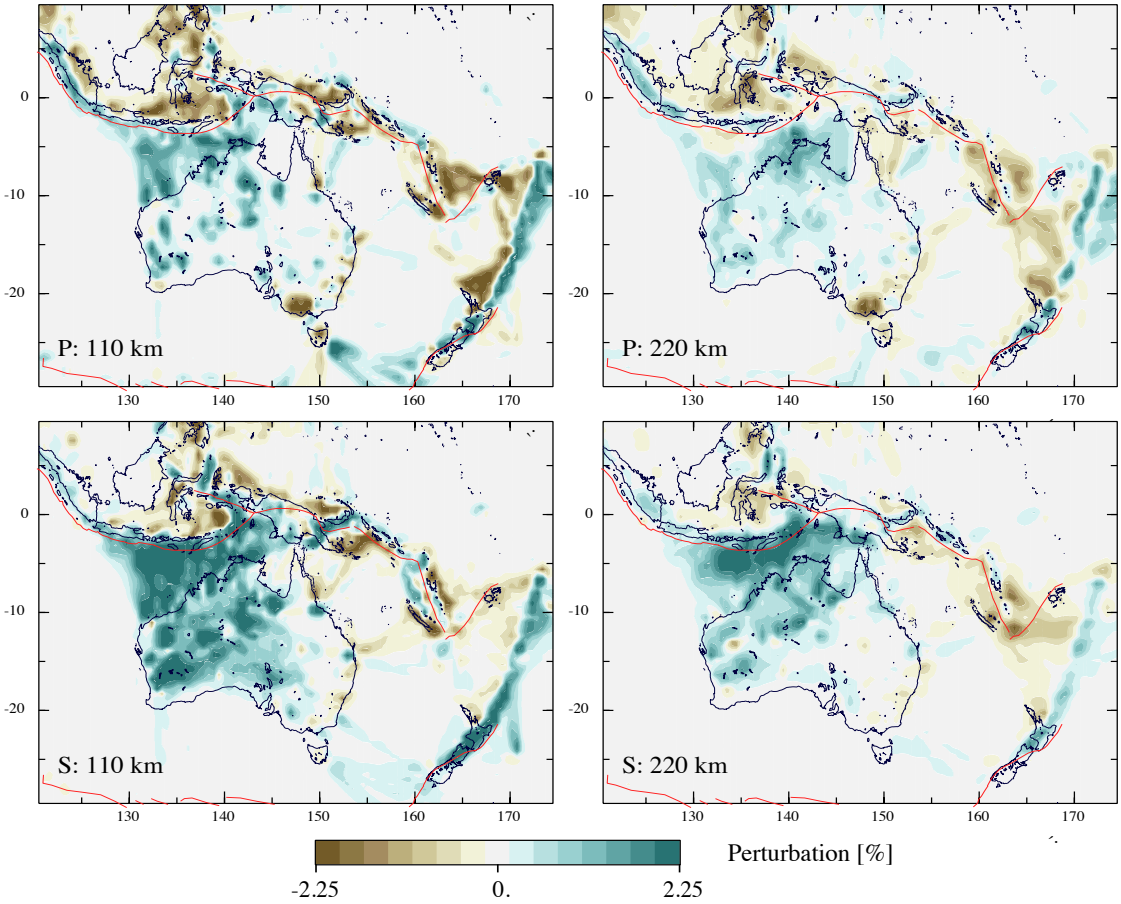

Figure 5. P and S wave tomography from body waves arrivals using the approach of Gorbatov & Kennett (2003). Slices are shown at 110 and 220 km to compare with Figures 3 and 4, allowing for the vertical stretching in the tomographic image. The images are displayed as perturbations from the *ak135* model of Kennett et al. (1995).

body waves means that the major features of the structure are well defined, and this forms the basis of our construction of the AuSREM mantle model. There are differences in smaller scale features and we anticipate that subsequent work will require revision in detail, but the present model should be a suitable starting point for, e.g., inversion for 3-D structure. Our primary source of information is for shear wavespeed, but we construct P wavespeed, density and attenuation models using information from body wave studies and petrological models.

The AuSREM mantle model is specified in terms of absolute velocities and densities since this is what is needed for many applications. The primary model nodes are at 0.5° spacing in latitude and longitude and 25 km spacing in depth from 75 – 300 km. A 50 km slice cuts the Moho in a few places across the continent (Kennett et al. 2011). Crustal influences on estimates of mantle structure are rather strong at this depth, but should be moderated by the way we have combined models with various approaches to the representation of crustal structure and consequently different crustal influences. To provide control at 50 km depth, we have combined the mantle SV model with a smoothed version of the S wave model from the crust (Salmon et al. 2012).

We start from three shear wavespeed models for the mantle in the Australian region based on very different approaches to the analysis of seismograms from regional earthquakes. We illustrate these models at depths of 100 km and 200 km in figures 3 and 4. We have used these shear wavespeed models as the primary information because they provide full continental coverage. The path coverage associated with each of the models is displayed in the Supplementary Material (Figure S-1). The disposition of available earthquakes means that path coverage drops off to the west of the Australian continent. The three models illustrated in Figures 3 and 4 use different approaches to the exploitation of seismic waveforms as well as different datasets. Nonetheless the broad outlines of the wavespeed structure are similar, and are in close concordance for the longer spatial wavelengths (Fichtner et al. 2012).

The first model is taken from Fishwick & Rawlinson (2012), building on the previous work of Fishwick et al., (2008), but with the inclusion of significantly more data. Path specific 1-D models are constructed using inversion for the fundamental Rayleigh mode and first few higher modes via the secondary variable approach of Cara & Lévêque (1987). The 1-D models are then combined in a linear inversion with regularisation to produce a series of depth slices at 25 km intervals. In this approach there is a strong influence from the fundamental Rayleigh mode and so sensitivity tends to diminish at depths below 250 km. The latest model exploits data from permanent and portable stations across both the Australian continent and the surrounding regions, resulting in over 13,000 paths included within the tomographic

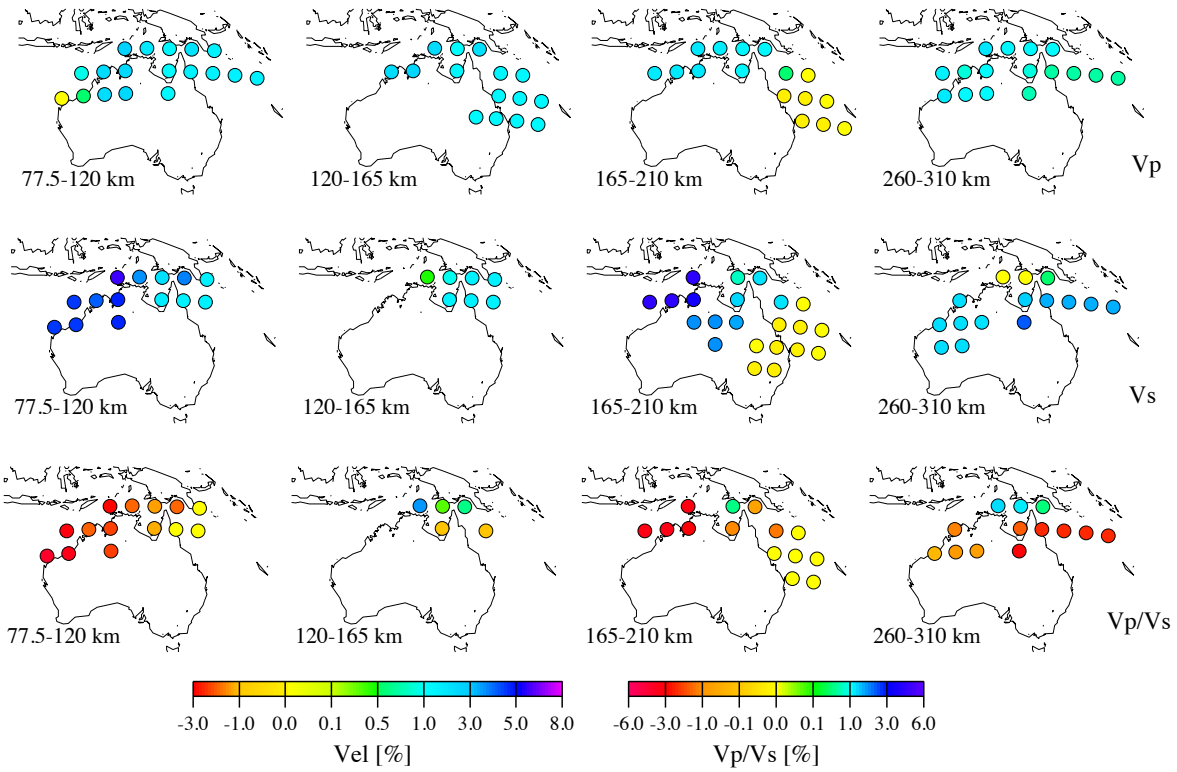

Figure 6. P and S wavespeed perturbations from the *ak135* model, and deviations in the P to S wavespeed ratio determined from studies of refracted body waves (Kaiho & Kennett, 2000).

inversion. Excellent path coverage and azimuthal distribution is observed in the centre and east of Australia, while the inclusion of Geoscience Australia stations has significantly improved coverage in the west (Fishwick & Rawlinson, 2012).

The second model is based on a 3-stage approach (Yoshizawa & Kennett 2004) with the inclusion of additional paths and allowance for radial anisotropy. A fully nonlinear waveform inversion is undertaken using the Neighbourhood Algorithm (Sambridge 1999). The criterion for matching the long-period multiple S waves and surface waves is based on a combination of envelope and phase fit in multiple time-frequency windows (Yoshizawa & Kennett 2002; Yoshizawa & Ekström 2010). Path-specific models from the nonlinear inversion are then interpreted as summaries of multi-mode dispersion. The reliability of estimated dispersion is evaluated by the relative modal strength and waveform fit in a time-frequency domain. A cluster analysis is then employed for eliminating outlying measurements (Yoshizawa & Ekström 2010), and eventually over 8000 paths for the fundamental mode and about 2000 paths for the higher modes are collected. For each mode a set of phase-speed maps are constructed as a function of frequency, incorporating possible off-great circle propagation and the influence zone around the propagation path which varies with frequency. Local dispersion curves are extracted and an inversion is made for a local 1-D model. Finally a 3-D model is assembled from the ensemble of local models.

The third model is taken from the work of Fichtner et al. (2010) where inversion for a radially anisotropic model is made using a linearised inversion with 3-D waveform modelling at each step, constructed using the spectral element method and an adjoint construction for the necessary derivatives for the frequency-time domain waveform fit criterion. A smooth 3-D starting model was based on the work of Fishwick et al. (2005) for wavespeeds and used the attenuation model presented in Kennett & Abdulah (2011). This is the most sophisticated and computationally intensive of the three methods and requires good calibration of the instrumental responses for the seismograms employed. More paths are brought in as the inversion proceeds so that the corresponding traces are sufficiently well represented that they can contribute to 3-D model improvement at the next iteration. Nevertheless the number of controlling paths (about 800) is less than in the other models, and azimuth control is limited on the western edge of the continent. Through fits to the multiple S phases (higher modes) the spectral element approach can provide information to considerable depth. Anomalies at 200 km and below tend to be somewhat larger than for the other methods, but the more limited sampling can induce quite strong local gradients, even though finite frequency effects are naturally included in the full 3-D inversion.

In addition to the differences in inversion methodology, the three models illustrated in figures 3 and 4 use different approaches to accounting for the crust, from path averages to a specially designed composite element for the spectral element method (Fichtner & Igel 2008). Nonetheless the broad outlines of the structure are similar, and the resemblances increase when appropriate spatial filtering is applied to extract the longer spatial wavelengths (Fichtner et al. 2012). In constructing the AuSREM mantle model we seek to produce a representation

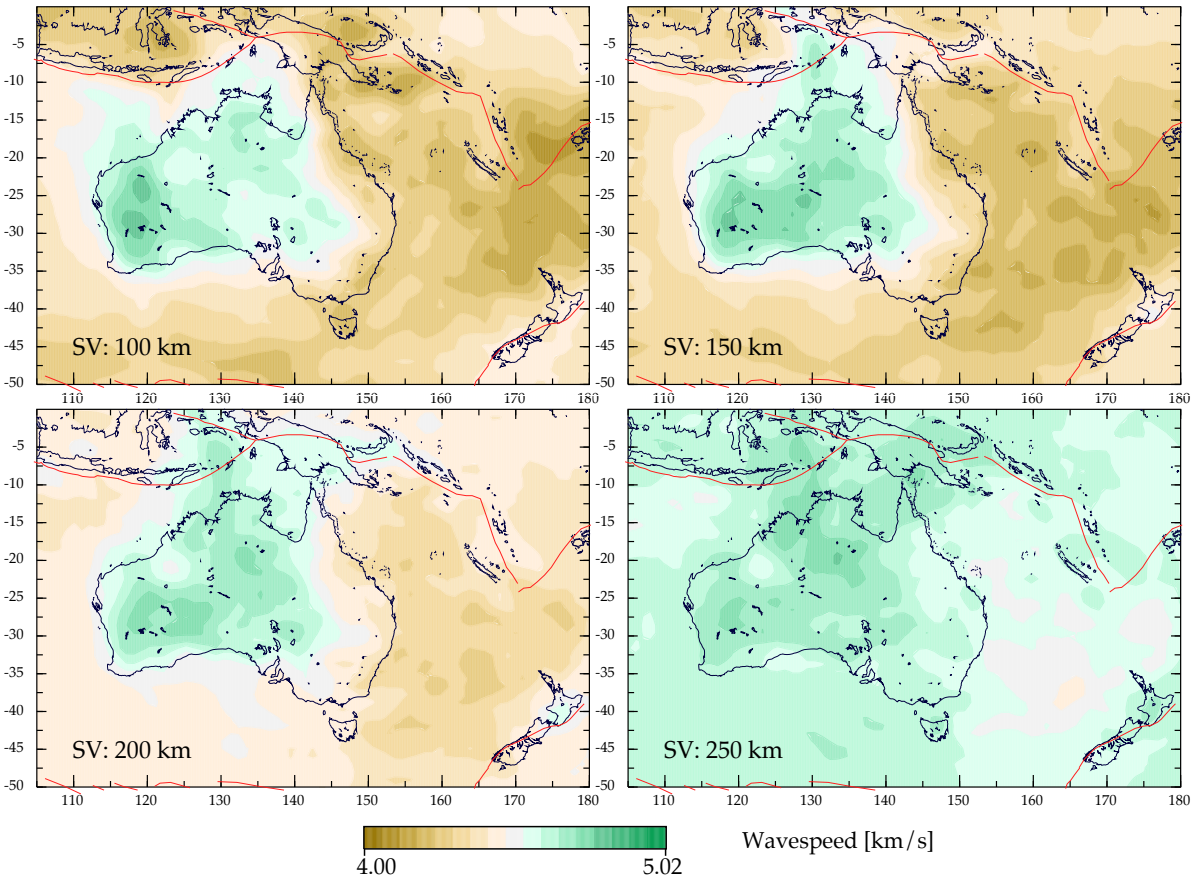

Figure 7. Slices through the AuSREM mantle model for SV wavespeed at: 100 km, 150 km, 200 km and 250 km depth.

where the major features are robust. We have therefore employed linear combinations of the shear wavespeed models to emphasise such features. Smaller scale features will tend to be suppressed even though they may be required, or introduced, by a particular data set and inversion scheme.

We have independent confirmation of the spatial configurations of fast and slower seismic wavespeeds from delay time tomography, which exploits teleseismic arrivals as well as those from regional events. In the absence of significant local events the majority of propagation paths travel rather steeply through the upper part of the mantle, and the attainable resolution is dictated by station coverage. In Figure 5 we show the results of P and S tomography using the approach described by Gorbatov & Kennett (2003). The results are displayed as deviations from the *ak135* model of Kennett et al. (1995). To allow for the stretching in the tomographic model induced by the narrow cone of sampling of the incident waves at the stations we present the images at 110 and 220 km for comparison with surface wave models at 100 and 200 km. This 10% correction gives a slight improvement in the correspondence between the two sets of results in the areas where we have adequate sampling. Localised station information, as in the the recent WOMBAT arrays in southeastern Australia for P waves, can bring in details that cannot be captured by the longer wavelengths employed in surface wave tomography (e.g. Fishwick & Rawlinson, 2012).

Additional valuable information on P wavespeed behaviour comes from the study of refracted body waves undertaken by Kaiho & Kennett (2000). They concentrated on a suite of corridors across the continent using events to the north and east of Australia, and were able to build corridor specific velocity models from analysis of the waveform, especially the nature of triplications arising from the upper mantle discontinuities. The wavespeeds from the various corridors were then brought together in a 3-D synthesis as illustrated in Figure 6. In addition we have assembled a set of travel time information for well-characterised paths traversing the Australian lithosphere for both P and S waves, building on the results of Kaiho & Kennett (2000) with later supplements (see Supplementary Material, Figures S-2, S-3). In particular, coverage of P waves is enhanced by studies of particularly well-located earthquakes undertaken by Geoscience Australia (S. Spiliopolous, personal communication).

P wavespeed variations from *ak135* are significantly smaller than for S. We use the information from the studies presented in Figures 5, 6, S-2, S-3 together with results from the tomographic study of Kennett & Abdulah (2011) to generate a suitable scaling relation between the wavespeed distributions. We have used a single relation for simplicity, in the absence of full control on the geographic variations in the P wavespeed distribution.

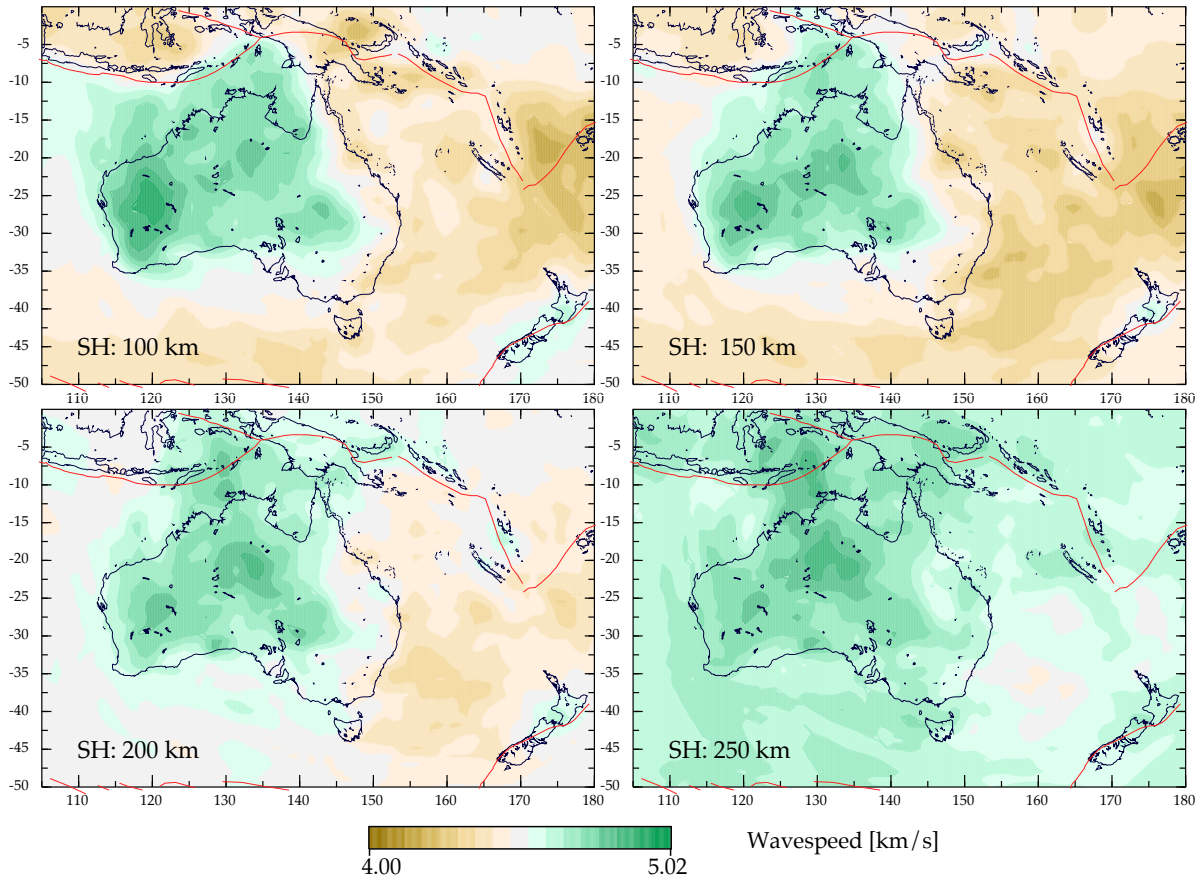

Figure 8. Slices through the AuSREM mantle model for SH wavespeed at: 100 km, 150 km, 200 km and 250 km depth.

3.1 Shear wavespeed

We have constructed a representative radially anisotropic model for the shear wavespeeds in the Australian mantle by using a weighted combination of the SV wave models and their SH wave counterparts, designed to also represent the body wave constraints. Our objective is to capture the main features of the lithosphere, and so by combining multiple models we reduce the dependence on the specific mode of inversion and the data coverage. As we have noted above, the longer spatial wavelength components of the three different studies are in good agreement as to the patterns of behaviour in the mantle, with fast S-wavespeeds in the west and centre of the continent and lower wavespeeds in the east and into the Tasman Sea. Differences in the size of the variations can be associated with the nature of the regularisation employed, and the influence of finite frequency. The construction of the composite model tends to suppress small-scale heterogeneities that are not well resolved. We recognise that a such a composite model need not provide as close a fit to a particular data set as provided by the model constructed directly from this dataset Yet, by virtue of having multiple sets of path coverage and different analysis techniques, the composite model tends to minimise the influence of minor features that may be dataset specific. Thus, the reference model should provide a good starting point for future inversions, because it emphasises the robust features of the structure beneath the continent and its environs.

There is considerable evidence for azimuthal anisotropy in the propagation of fundamental mode Rayleigh waves across the Australian continent (e.g., Debayle et al. 2005; Fishwick et al. 2008) with a change in dominant fast wavespeed direction from east-west at 100 km depth to nearly north-south at 200 km depth. Such studies suggest that less than 15% of the total variation in SV wavespeed could be attributable to azimuthal variation. We have decided against trying to include such azimuthal effects in the reference model. To do so in a fully consistent way would require a rather complex anisotropic model that would be very difficult to use for general purposes. We have, however, incorporated polarisation anisotropy with separate SV and SH wave models, equivalent to transverse isotropy with a vertical symmetry axis.

The reference model is based on the suite of models displayed in Figures 3 and 4 taken in conjunction with the body wave results. The latest shear wavespeed models from waveform inversion incorporate more of the Geoscience Australia permanent stations and portable stations deployed since the earlier studies (Fishwick et al. 2008, Yoshizawa & Kennett 2004). These updates significantly improve the path coverage, especially in the west, see Figure S-1. The models are used without spatial filtering, and we construct a weighted sum. We have given modest emphasis to the studies with the highest path density, whilst recognising the benefits arising from improved representations of finite-frequency and 3-D effects. A number of candidate models were prepared and the selection of the reference was made based on preferred character across the range of depths, and compatibility with body wave constraints where they are available. Any process of selecting weights

between different models will have some subjective component, but our aim has been to produce a representative model that is generally smooth and captures the main long wavelength features, yet presents detail where the diverse models and data sources concur.

The final weighting for the SV wavespeed reference model $\beta^{\mathrm{V}}_{\mathrm{ref}}$ at depths from 75–300 km is

$$\beta^{\mathrm{V}}_{\mathrm{ref}}(z) = 0.38\beta^{\mathrm{V}}_{\mathrm{F}}(z) + 0.37\beta^{\mathrm{V}}_{Y}(z) + 0.25\beta^{\mathrm{V}}_{W}(z), \tag{1}$$

where β_{F} is the updated Fishwick model, β_Y is the updated Yoshizawa model, and β_W comes from the full-waveform inversion of Fichtner et al. (2010).

The SV model is well constrained and we can have considerable confidence in the main features (Figure 7). The principal differences in the constituent models arise in variability in the shallower parts of the mantle near the western margin of Australia, where path sampling is both less and also less well distributed azimuthally (see Figure S-1). The AuSREM mantle representation is designed to cover the full range of seismic frequencies and so the choice of model combinations has been guided by consistency with body wave results (as in Figures 5, 6, S-2, S-3). We recognise that there will be modifications needed in the future in the light of new information. Indeed a major role for a reference model is to assist in the development of such new studies.

We have less control on the SH wave distribution, and in this case we have to recognise that there are some discrepancies between the base models. Nevertheless, we feel that the SH model illustrated in Figure 8 is suitably representative of the main features of the wavespeed in 3-D. This SH reference model $\beta^{\mathrm{H}}_{\mathrm{ref}}$ has been constructed with the weighting

$$\beta^{\mathrm{H}}_{\mathrm{ref}}(z) = 0.6\beta^{\mathrm{H}}_{Y}(z) + 0.4\beta^{\mathrm{H}}_{W}(z), \tag{2}$$

which places greater emphasis on the model with broader path coverage particularly in the west, but allows detail to be introduced from the full waveform-inversion study.

The SH model displayed in Figure 8 uses direct information from the prior models, but tends to have shorter wavelength features than the SV model. In consequence the distribution of the SH/SV wavespeed ratio between the models shown in Figures 8 and 7 is rather patchy. In the Appendix we present an alternative construction for an SH model utilising a smooth SH/SV ratio.

3.2 P wavespeed

The main information we have on the P wavespeed distribution comes from refracted waves and body-wave tomography. The variations in P wavespeed in the cratonic lithosphere of Australia are typically between a half and one third of the corresponding S variations from the *ak135* model. This provides a useful starting point, but we have been able to incorporate lateral variability in the $V_{\mathrm{p}}/V_{\mathrm{s}}$ ratio to allow for differences between the zones beneath the cratons and the Phanerozoic fold belts. We also have some hints of age dependence between the Archæan and Proterozoic domains.

Building on the results of Kaiho & Kennett (2000), we have represented the variations in the $V_{\mathrm{p}}/V_{\mathrm{s}}$ ratio by scaling the relative deviations $\delta \ln \beta$ in SV wavespeed from the *ak135* model to produce corresponding P wavespeed deviations $\delta \ln \alpha$:

$$\begin{aligned} \delta \ln \alpha &= \delta \ln \beta / [1.875 + (\delta \ln \beta - 0.01) * 20.0], \qquad \delta \ln \beta > 0.01, \\ &= \delta \ln \beta / [1.875 + (\delta \ln \beta - 0.01) * 2.50], \qquad \delta \ln \beta < 0.01. \end{aligned} \tag{3}$$

Then the absolute P wavespeed is constructed from

$$\alpha = \alpha_0(1 + \delta \ln \alpha), \tag{4}$$

where α_0 is the value for the *ak135* model. This simple scheme goes a long way towards capturing the strong effects on P wavespeed in areas of reduced S wavespeed, and the somewhat muted variations in P wavespeed in the higher S wavespeed zones.

The resulting P wavespeed distribution is shown in Figure 9 for the same set of depth slices employed for the SV and SH waves (Figures 7 and 8). At 100 km depth the lowered wavespeeds in the Tasman Sea are prominent. The contrast with the continent diminishes with depth.

3.3 Density

We have less direct information on the density in the mantle, apart from the study of Aitken (2010) in which gravity inversion with seismic constraints was used to produce a model of the Moho across Australia. Airy compensation from a depth close to 60 km is largely compatible with the surface gravity results and so we do not need to invoke significant density variations in the upper mantle.

However, if we adopt a simple wavespeed-density scaling we will require large densities for the thick cratons, that are incompatible with their buoyant nature in the mantle. Guided by density estimates for different compositions from highly refractory harzburgite to more fertile configurations (S. Klemme, personal communication), we have constructed an empirical shear-wavespeed density relation that compensates for the high cratonic wavespeeds in the lithosphere. We set a threshold for the transition to the inclusion of a compositional effect at depth z: $\epsilon = 2.0 + 0.2 * (z - 50)$ percentage deviation in shear wavespeed from the *ak135* model. If the shear wavespeed perturbation at a particular depth is less than $\epsilon\%$, we use a simple scaling of the variation to produce the local density

$$\rho = \rho_0(1 + 0.3 * \delta \ln \beta), \tag{5}$$

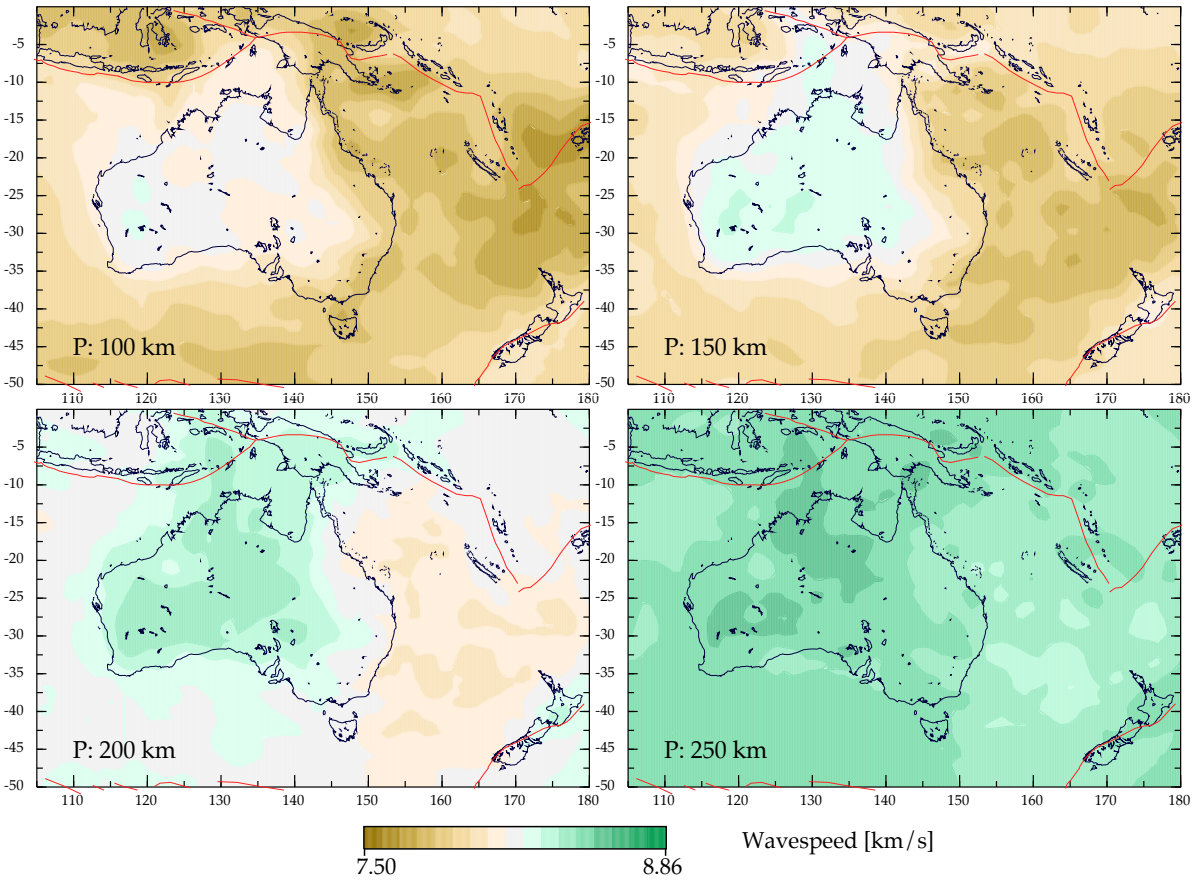

Figure 9. Slices through the AuSREM mantle model for P wavespeed at: 100 km, 150 km, 200 km and 250 km depth.

where ρ_0 is taken from *ak135*. For larger perturbations we use a relation with an inverse slope in terms of the absolute SV wavespeed β,

$$\rho = (13.931 - \beta)/2.7724. \quad (6)$$

Below 180 km we scale back the reduction in density linearly with depth, so that a single representation is applied at 300 km depth.

The two representations link well and we do not see very much of an outline of the fast wavespeed zones in the results for density (Figure 10) except at 200 km where we can readily identify the zone of likely compositional heterogeneity. As can be seen in the plots of the resulting density distribution in Figure 10, the density contrasts in the mantle are modest and compatible with some degree of thermal input in, e.g., the Tasman Sea.

3.4 Transition to the Asthenosphere

We can readily recognise the lithosphere beneath the older parts of the continent by fast shear wavespeeds (up to 4.7 km/s), but the transition to the asthenosphere beneath is not generally marked by any sharp transition. Rather there is a gradation from a conductive to a convective regime, most likely linked also to a change in rheology from dislocation to diffusion creep. The presence of the asthenosphere is, however, manifest in enhanced seismic attenuation. The fast lithospheric wavespeeds are accompanied by little loss of seismic energy, enabling high frequency waves for both P and S to propagate readily from subduction zones into continental Australia (Kennett & Furumura 2008) with extended scattered codas. The high frequency S waves are suddenly lost when the seismic waves penetrate into the asthenosphere, because of its much higher attenuation of shear waves than in the lithosphere (Gudmundsson et al. 1994). The effect on P waves is significant with a strong change in frequency content, but not as dramatic as for S. Kennett & Abdulah (2011) have used the full range of P and S wave arrivals at portable stations across Australia to undertake attenuation tomography that confirms the presence of much stronger attenuation below 210 km depth. Unfortunately we are not able to distinguish between a thin zone of very high attenuation and a broader zone with a less attenuation; so such studies can only provide a broad scale picture of the behaviour.

Based on the concept of the transition from a conductive to convective regime we can expect to seek evidence for the transition to the asthenosphere through changes in wavespeed gradient. In the absence of a single criterion we have found it effective to use multiple estimators for the location of the base of the lithosphere including the analysis of refracted waves in the mantle, and the wavespeeds and gradients deduced from surface-wave tomography and body-wave tomography. The resulting estimate of the depth to the lithosphere-asthenosphere

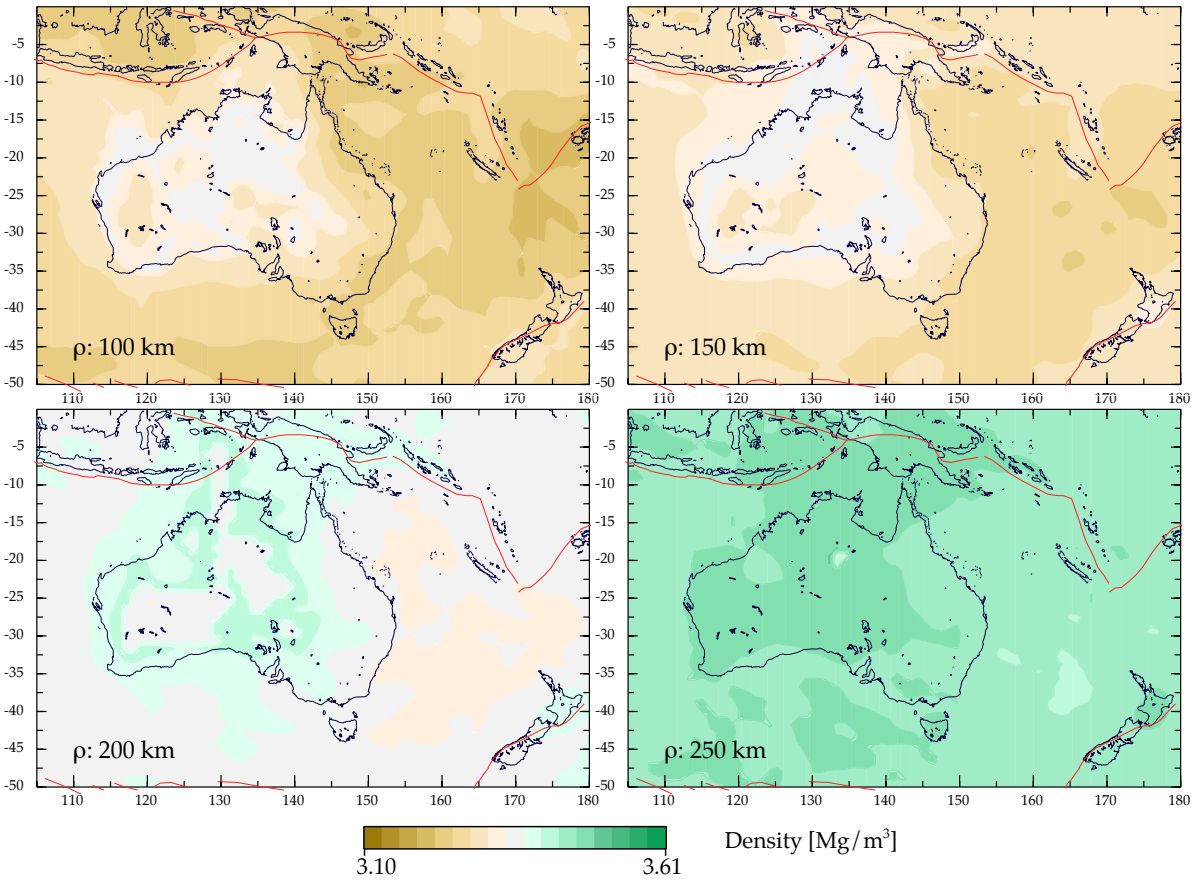

Figure 10. Slices through the AuSREM mantle model for density at: 100 km, 150 km, 200 km and 250 km depth.

transition is shown in Figure 11. The relative variations in the thickness of the lithosphere should be reliable, but the absolute values depend on exactly where the boundary is drawn in a gradational transition. Only in eastern Australia, where the lithosphere is thin, is there S receiver function evidence for a rapid wavespeed change (Ford et al. 2010). Structure in central Australia is complex, and the gradation of structure with depth is somewhat different than in the rest of the continent (see, e.g., the cross-sections in Figure 13). It is hard to tell whether, or not, there are localised patches of rather deep penetration of lithospheric material.

The contrast between thick lithosphere in the centre and west and thinner lithosphere in the east is very clear in Figure 11. The nature of the transition from west to east is consistent with the analysis of Fishwick et al. (2008), and it appears that changes in lithosphere thickness can occur over quite narrow zones. Our estimates of the depth to the base of the lithosphere show significant irregularities. This irregular base is likely to impose complex stress patterns in both the lithosphere and asthenosphere associated with the relative motions of the thick continental lithosphere and the freer-flowing asthenosphere. The presence of lithospheric 'steps' will produce complex flows and this has lead Farrington et al. (2010) to suggest an edge convection model for the formation of the Newer Volcanic province in Victoria and South Australia that host the most recent eruptions at 4.6 ka. Their concept is that the northward motion of Australia at about 7 cm/yr gives rise to a trailing flow from the southern edge of the thick cratonic lithosphere that comes to the surface further south creating the volcanic province.

3.5 Attenuation

We have constructed an S wave attenuation model to accompany the wavespeed distribution. This Q_β^{-1} model incorporates the very low loss of seismic energy in the cratonic lithosphere (cf. Kennett & Furumura, 2008), and enhanced asthenospheric loss. We use a single S wave attenuation model. Even though we would expect equivalent polarisation anisotropy in attenuation to wavespeeds, the differences are rather small (Kennett & Abdulah 2011). The studies of Adbulah (2007) show that the frequency dependence of Q_β^{-1}, at 1 Hz and below, is slight with a frequency exponent less than 0.1, except in the shallow areas of strong attenuation such as the Coral Sea. We have therefore adopted a frequency independent attenuation model. P wave attenuation is well represented by a simple scaling $Q_\alpha^{-1} = 0.5 * Q_\beta^{-1}$.

The attenuation tomography undertaken by Kennett & Abdulah (2011) has highest resolution in the northern part of Australia and towards the Indonesian subduction zone. This model provides important constraints, but the use of stations confined to the continent means that coverage is limited to the east into the Tasman Sea, where surface wave results (Dalton et al. 2008) indicate enhanced attenuation ($Q_\beta^{-1} > 0.03$). We have therefore made use of the strong correlation between reduced seismic wavespeeds and enhanced attenuation due

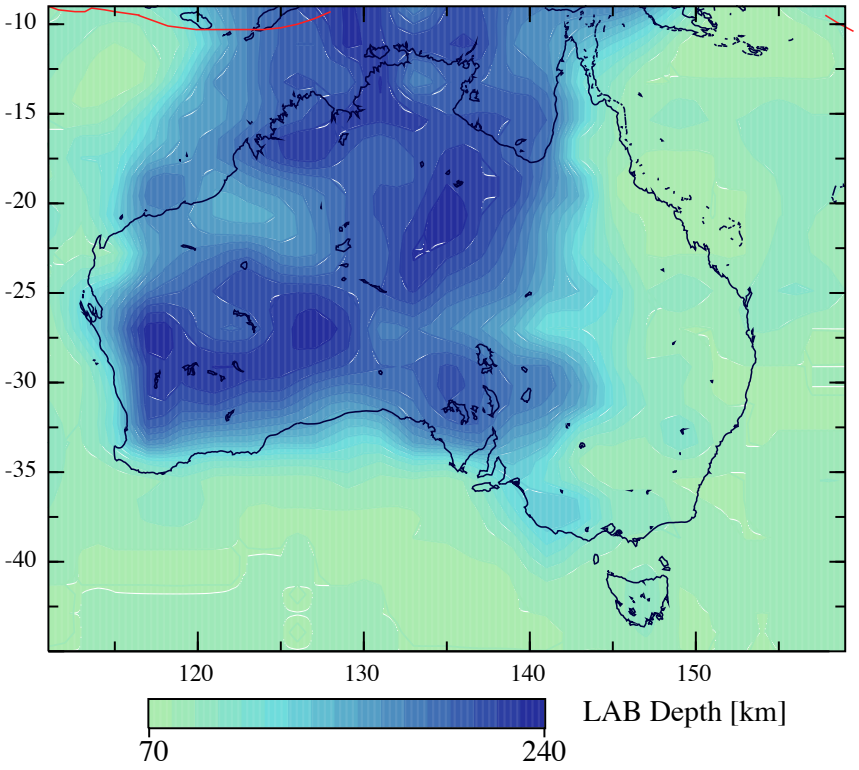

Figure 11. Estimate of the depth to the Lithosphere-Asthenosphere boundary derived from a combination of different lines of evidence including absolute wavespeed and both horizontal and vertical wavespeed gradients

to the influence of increased temperature or volatiles. The very high S wavespeeds found in the cratonic mantle are very hard to explain with temperature alone, and correlate very well with efficient transmission of high frequency energy from the subduction zones to the north (Kennett & Furumura 2008).

We have therefore made the assumption that a 4% positive perturbation from the *ak135* reference model is associated with $Q_{\beta 0}^{-1} = 0.001$ (i.e., $Q_{\beta 0} = 1000$) within the lithosphere. Down to 200 km depth we then construct the S wave attenuation factor at a horizontal position $\mathbf{x}$ and depth z as

$$Q_\beta^{-1}(\mathbf{x}, z) = Q_{\beta 0}^{-1} \exp\{\zeta[0.04 - \Delta_r\beta(\mathbf{x}, z)]\}, \quad z \leq 200 \text{ km}, \tag{7}$$

where $\Delta_r\beta(\mathbf{x}, z) = [\beta(\mathbf{x}, z) - \beta_0(z)]/\beta_0(z)$ with $\beta_0(z)$ taken from the *ak135* model. Seismic loss then increases rapidly for strong negative $\Delta_r\beta$. The functional relation (7) represents the even faster increase of seismic attenuation than decrease in seismic wavespeed as the solidus is approached (Faul & Jackson, 2005). The scaling factor ζ has been tuned to match the northern Australian results of Kennett & Abdulah (2011). We have adopted the value $\zeta = 19.0$, which means that seismic attenuation increases 10 fold to $Q_{\beta 0}^{-1} = 0.01$ (i.e., $Q_{\beta 0} = 100$) for a perturbation of -8.12% from *ak135*. In the asthenospheric zone below 200 km, we shift the reference and now require a 10% positive deviation from *ak135* to correspond to $Q_{\beta 0}^{-1} = 0.001$; this corresponds to the change in grain size invoked by Faul & Jackson (2005). The loss factor is then

$$Q_\beta^{-1}(\mathbf{x}, z) = Q_{\beta 0}^{-1} \exp\{\zeta[0.10 - \Delta_r\beta(\mathbf{x}, z)]\}, \quad z > 200 \text{ km}, \tag{8}$$

with the same scaling factor ζ as before.

This simple empirical scheme reproduces well the attenuation patterns across the Australian continent found by Kennett & Abdulah (2011), yet allows them to be expanded to the full domain of the AuSREM mantle model. In Figure 12 we show the Q_β^{-1} attenuation distribution derived from the SV wavespeed model, for the same set of depth slices as we have used for the other physical parameters.

The strong contrast in seismic attenuation between the cratonic core and the eastern margin of Australia is evident in the 100 km slice. The centres of attenuation on the continent in northern Queensland and Victoria link to recent volcanism. The north Queensland anomaly extends into the Coral Sea, a prominent feature in the Kennett & Abdulah (2011) results. There is strong shallow attenuation in the east, notably beneath the Lau Basin, a location of active spreading where $Q_\beta^{-1} > 0.0125$ (i.e. $Q_\beta < 80$) as would be expected in such a hot environment, and in agreement with previous body wave studies (e.g., Flanagan & Wiens, 1998; Roth et al., 1999). At 150 km depth we see the strong cratonic zone of low loss, bordered to the east by a well developed higher attenuation corridor and a shallower asthenosphere

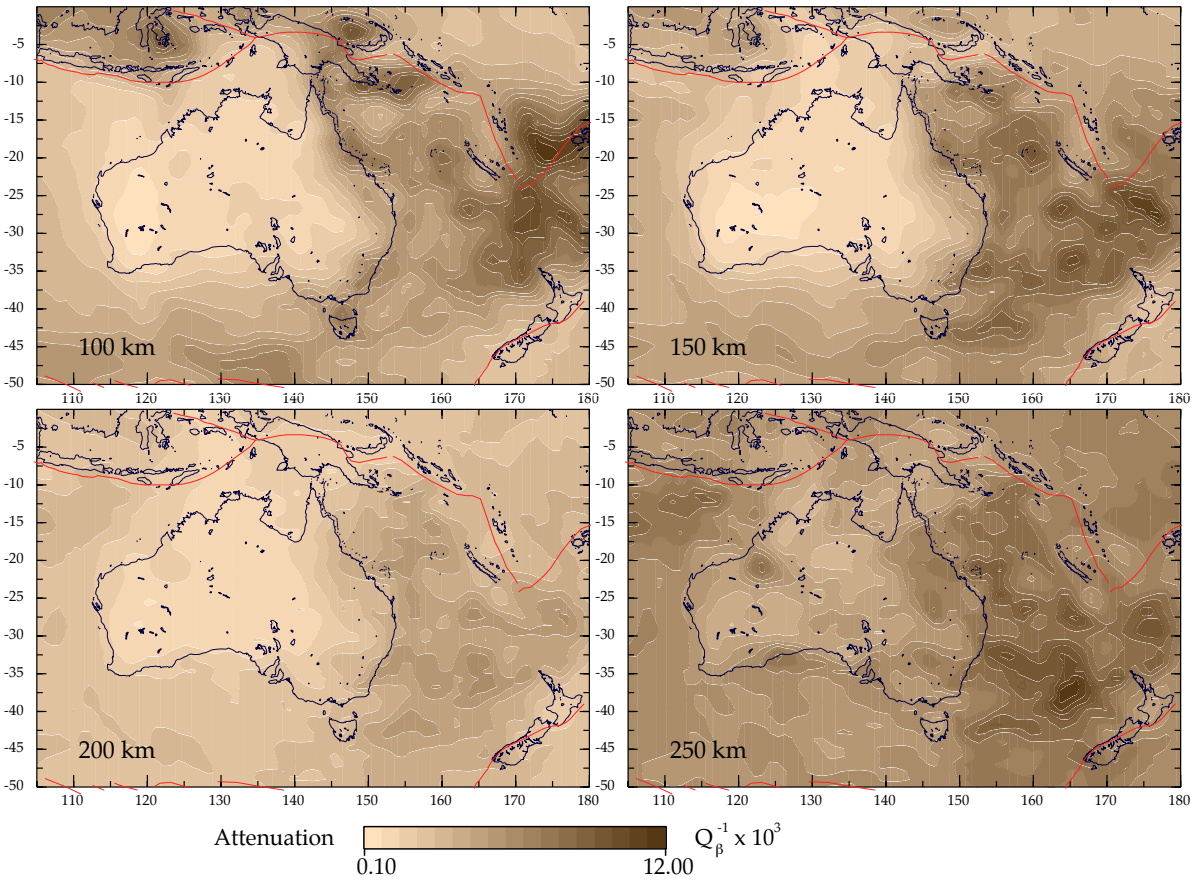

Figure 12. Slices through the AuSREM attenuation model at: 100 km, 150 km, 200 km and 250 km depth.

consistent with early surface wave studies, e.g., Goncz & Cleary (1976). At greater depth we see a shift of the whole attenuation distribution to much larger loss of seismic energy, with only a few pockets of lower attenuation associated with cratonic roots (cf. Figure 11).

3.6 External domain

Outside the zone covered by the AuSREM mantle model, we employ the model S40RTS of Ritsema et al. (2011). Within our model zone the patterns of variation in S40RTS are compatible with the larger wavelength features of our model, but the range of wavespeeds is somewhat smaller. We have therefore engaged in gentle tapering at the edges of the AuSREM model to ensure a smooth transition into S40RTS.

4 DISCUSSION AND CONCLUSIONS

The AUSREM mantle model attempts to provide a representation of the complex pattern of 3-D structure beneath the Australian Plate. The construction of the model has endeavoured to bring in different styles of modelling and inversion, so that the distinctive features of the mantle in the Australian region are adequately captured. For this AuSREM mantle component we use the SV wavespeed as the primary control, and have derived the P wavespeed, density and shear attenuation from this field. Although we have made a direct construction of an SH model, we present an alternative, smoother model derived from the SV model in the Appendix.

The most prominent feature of the mantle model is the presence of fast shear wavespeeds in the west and centre of Australia compared with the east. This has been a consistent feature as models for the lithospheric mantle under Australia have developed (e.g. Kennett 2003). As can be seen in Figures 3 and 4 this is a a common feature of the three shear wavespeed models we have used, and also appears in global models such as S40RTS (Ritsema et al. 2011) though there the resolution is less.

The effect of increasing temperature is to lower seismic wavespeeds. In consequence much of the pattern of wavespeeds can be explained by temperature alone, especially where wavespeeds are low. Goes et al. (2005) attempted to extract temperature from the SV wavespeed model of Yoshizawa & Kennett (2004), and were forced to very low temperatures ($< 500^\circ$C) in the centre and west, with a very large temperature contrast ($> 1000^\circ$C) to the hotter region beneath the Tasman Sea. The exceptionally high wavespeeds for SH in AuSREM suggest that, as in the study of N. America by Khan et al. (2011), compositional heterogeneity is required to achieve the highest shear velocities. This would

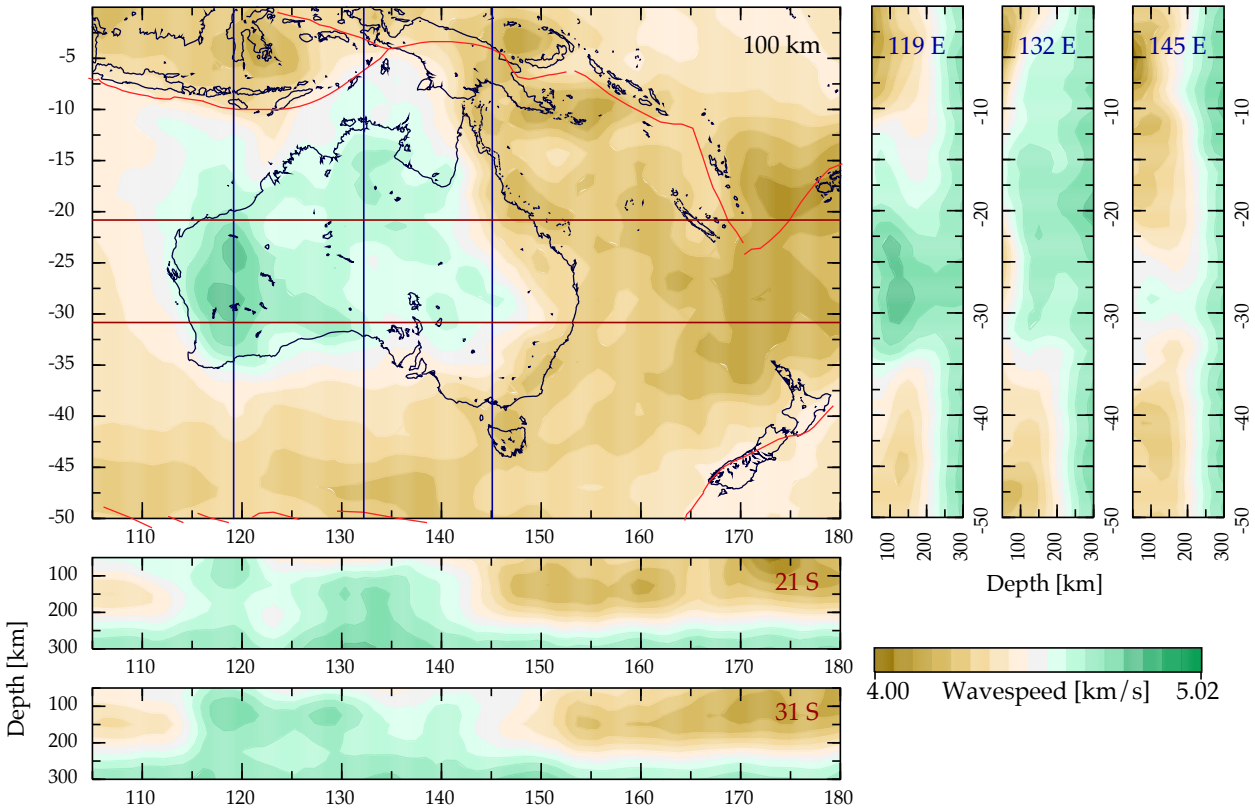

Figure 13. Cross-sections through the SV wavespeed component of the AuSREM mantle model. along the lines indicated on the key map showing the a map view at 100 km depth. Sections are shown at 21°S, 31°S and at 119°E, 132°E, 145°E. Note, as in the depth slices, the colours represent absolute wavespeed so that an increase with depth is to be expected.

also be consistent with the very low attenuation observed on paths in cratonic Australia. The lightest tones in the attenuation model in Figure 12 can thus be expected to outline the area where compositional heterogeneity dominates.

The most common compositional explanation for high seismic velocities is an increase in the Mg#. In central and western Australia this would be quite consistent with the patterns of geochemical variation inferred from inversion of multi-mode surface wave dispersion for Australia (A. Khan – personal communication). However, it is not clear that a change in Mg# can account for the magnitude of seismic velocity anomaly observed in the reference model. A recent study on the effect of polybaric partial melting indicates maximum V_s increases of 1.7%, and only for deep melting paths or high potential temperatures (Afonso & Schutt, 2012). These results are in line with previous studies that show the range of velocity variation due to melt depletion to be small, and comparable to the uncertainties in the seismic velocities themselves (e.g. Goes et al., 2000). Therefore, while melt depletion is likely to play some role in the high velocities observed beneath much of central and western Australia, further investigation into the maximum amplitude of velocity anomalies is required.

The nature of the mantle model is illustrated in Figure 13 which shows a group of selected cross-sections through the SV wavespeed distribution in both longitude and latitude keyed to a map view at 100 km depth. As in the earlier images we work with absolute velocities, so that there is a natural tendency for the wavespeed to increase with depth. Figure 13 shows very clearly the ambiguities inherent in the choice of a base of the lithosphere. vertical gradients are rather variable, and a criterion that would be very suitable for Western Australia might well be less appropriate for the complex structures in central Australia.

Despite the problems of definition we can recognise a broad pattern in lithospheric thickness that is insensitive to the particular definition employed for the lithosphere-asthenosphere boundary (cf. Figure 11). The cratonic region in the centre and west of Australia is underlain by a thick mantle lithosphere extending to over 200 km depth with fast wavespeeds (especially for shear waves). Beneath the Tasman Fold Belt in the east, a region of younger Phanerozoic upper crust, the lithosphere is generally thinner (less than 140 km) and the asthenosphere has a pronounced low velocity zone for shear waves with high attenuation of shear wave energy.

The centre of Australia has relatively low wavespeeds at 75 km (Figures 13, 14), but there are strong gradients with depth and by 125 km a broad zone of fast wavespeeds is established across the centre and west of Australia that persists to more than 200 km depth (Figures 5, 11, 13). Lower seismic wavespeeds are also seen in the Canning Basin area to some depth. These are the two regions that have seen the most recent deformation. Elsewhere, the ancient continental core of Australia in the centre and west of the continent is marked by relatively high seismic wavespeeds throughout the lithosphere (Figure 14).

In contrast in the Tasman Fold belt to the east, the seismic wavespeeds in the mantle are somewhat lower and the lithosphere is relatively

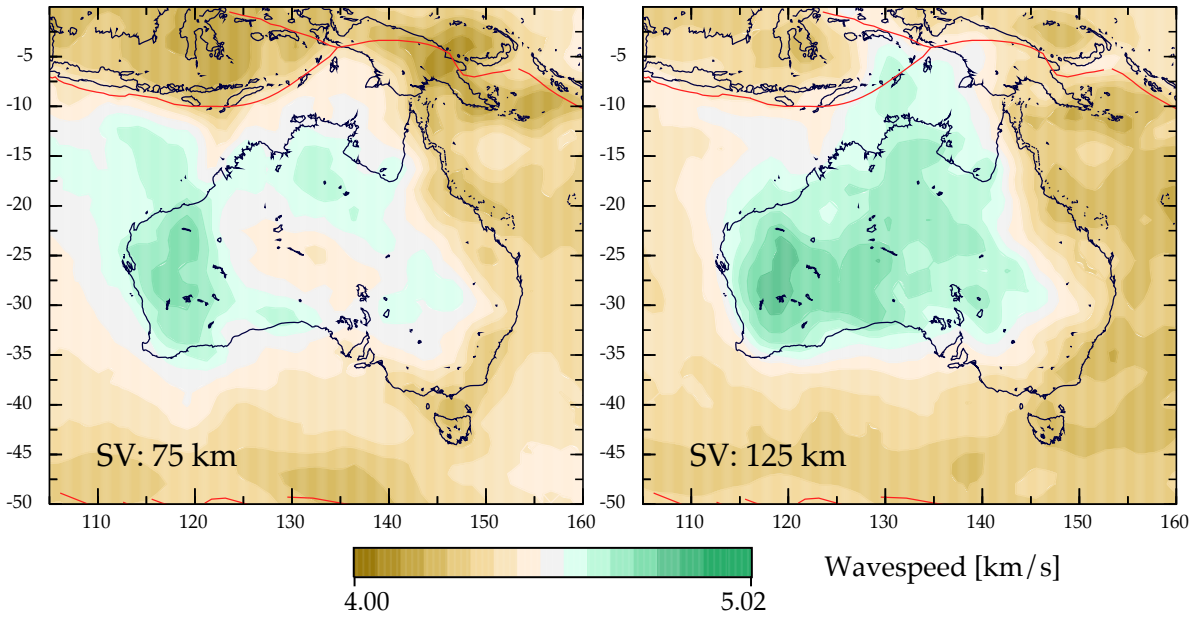

Figure 14. Comparison of SV wavespeed at 75 km and 125 km depth.

thin, with estimates around 80 km. The Tasman Sea region displays quite low shear wavespeeds (down to 4.2 km/s), probably as a result of residual heat left from failed rifting around 80 Ma (Figure 13). Fishwick et al. (2008) have presented evidence for the progressive eastward thinning of the lithosphere across Australia, which occurs as a series of discrete steps with quite sharp transitions. This result poses interesting questions as to how such lithospheric steps can be maintained over extended periods of geological time.

The complete AuSREM model with both crustal and mantle provides a representation of 3-D structure beneath Australia and its environs at a common 0.5 degree sampling that can be used for many purposes. Both the crustal and mantle components should be useful in gravity modelling and in studies of dynamic topography. The crustal component provides corrections for future mantle studies for both surface wave tomography and delay time tomography on a finer scale. Tools are under active development for location of earthquakes in the full 3-D model, and for earthquake source characterisation.

5 THE AUSREM MODEL

The AuSREM model is presented in full at the web-site
http://rses.anu.edu.au/seismology/AuSREM
from which the model can be downloaded in a number of formats, and where it is also possible to generate maps and depth profiles.

ACKNOWLEDGEMENTS

The AuSREM project has been jointly supported by AuScope and the Research School of Earth Sciences, Australian National University. Funding support for the passive seismic work in Australia has been provided from the Australian National University, from Discovery Projects funded by the Australian Research Council, from the Predictive Mineral Discovery Cooperative Research Centre, and the AuScope infrastructure initiative. Prof S. Klemme is thanked for discussions on mantle density.

REFERENCES

Abdulah, A., 2007. *Seismic Body Wave Attenuation Tomography beneath the Australasian region*, Ph.D. Thesis, Australian National University.

Afonso, J.C. & Schutt, D.L. 2012. The effects of polybaric partial melting on density and seismic velocities of mantle restites, *Lithos*, **134–135**, 289–303.

Aitken, A.R.A., 2010. Moho Geometry Gravity Inversion Experiment (MoGGIE): A refined model of the Australian Moho, and its tectonic and isostatic implications, *Earth Planet. Sci. Lett.*, **297**, 71–83.

Cara, M. & Lévêque, J., 1987. Waveform inversion using secondary observables, *Geophys. Res. Lett.*, **14**, 1046–1049.

Dalton, C.A., Ekström, G. & Dziewoński, A.M.. 2008. The global attenuation structure of the upper mantle, *J. Geophys. Res.*, **113**, B09303, doi:10.10292007JB005429.

Debayle, E. & Kennett, B.L.N. 2003, Surface wave studies of the Australian region, 25–40, in *The Evolution and Dynamics of the Australian Plate*, Ed. D. Müller & R. Hillis. Geological Society of Australia Special Publication **22** and Geological Society of America Special Paper **372**.

Debayle, E., Kennett, B.L.N. & Priestley, K., 2005. Global azimuthal seismic anisotropy and the unique plate-motion deformation of Australia, *Nature*, **433**, 509–512.

Farrington R., Stegman D., Moresi L.N., Sandiford M. & May D., 2010. Interactions of 3D mantle flow and continental lithosphere near passive margins. *Tectonophys.*, **483**, 20–28.

Faul, U. & Jackson, I., 2005. The seismological signature of temperature and grain size variations in the upper mantle, *Earth Planet. Sci. Lett.*, **234**, 119–234.

Fichtner, A. & Igel, H., 2008. Efficient numerical surface wave propagation through the optimization of discrete crustal models: a technique based on non-linear dispersion curve matching (DCM), *Geophys. J. Int.*, **173**, 519–533.

Fichtner, A., Kennett, B.L.N., Igel, H. & Bunge, H.-P., 2009. Full seismic waveform tomography for upper-mantle structure in the Australasian region using adjoint methods, *Geophys. J. Int.*, **179**, 1703–1725.

Fichtner, A., Kennett, B.L.N., Igel, H. & Bunge, H.-P., 2010. Full seismic waveform tomography for radially anisotropic structure: New insights into the past and present states of the Australasian upper mantle, *Earth Planet. Sci. Lett.*, **290**, 270–280.

Fichtner, A., Fishwick, S., Yoshizawa, K. & Kennett, B.L.N., 2012. Optimal spherical spline filters for the analysis and comparison of regional-scale tomographic models, Phys. Earth Planet. Inter., **190**, 44–50.

Fishwick, S., Kennett, B.L.N. & Reading, A.M., 2005. Contrasts in lithospheric structure within the Australian Craton, *Earth Planet. Sci. Lett.*, **231**, 163–176.

Fishwick, S., Heintz, M., Kennett, B.L.N., Reading, A.M. & Yoshizawa, K., 2008. Steps in lithospheric thickness within eastern Australia, evidence from surface wave tomography, *Tectonics*, **27**, TC0049, doi:10.129/2007TC002116.

Fishwick, S. & Reading, A.M., 2008, Anomalous lithosphere beneath the Proterozoic of western and central Australia: A record of continental collision and intraplate deformation? *Precambrian Res.*, **166**, 111–121.

Fishwick S. & Rawlinson N., 2012. 3-D structure of the Australian lithosphere from evolving seismic datasets, *Aust. J. Earth Sci.*, **59**, 809–826.

Flanagan, M.P. & Wiens, D.A., 1998. Attenuation of broadband P and S waves in Tongas: Observations of frequency dependent Q, *Pure and Applied Geophysics*, **153**, 345–375

Ford, H.A., Fischer, K.M., Abt, D.L., Rychert, C.A. & Elkins-Tanton, L.T., 2010. The lithosphere-asthenosphere boundary and cratonic lithospheric layering beneath Australia from *Sp* wave imaging, *Earth Planet. Sci. Lett.*, **300**, 299–310.

Goncz, J.H. & Cleary, J.R., 1976. variations in the structure of the upper mantle beneath Australia, from Rayleigh wave observations, *Geophys. J. R. Astr. Soc.*, **44**, 507–516.

Goes, S., Govers, R., Vacher, P., 2000. Shallow mantle temperatures under Europe from P and S wave tomography. *J. Geophys. Res.*, **105**, 11153–11169.

Goes, S., Simons, F.J., Yoshizawa, K., 2005. Seismic constraints on temperature of the Australian uppermost mantle. *Earth Planet. Sci. Lett.*, **236**, 227–237.

Gorbatov, A. & Kennett, B.L.N., 2003. Joint bulk-sound and shear tomography for Western Pacific subduction zones, *Earth Planet. Sci. Lett.*, **210**, 527–543.

Gudmundsson, O., Kennett, B.L.N. & Goody, A., 1994. Broadband observations of upper mantle seismic phases in northern Australia and the attenuation structure in the upper mantle, *Phys. Earth Planet. Inter.*, **84**, 207–236.

Kaiho, Y. & Kennett, B.L.N., 2000. Three-dimensional seismic structure beneath the Australasian region from refracted wave observations, *Geophys. J. Int.*, **142**, 651–668.

Kennett, B.L.N. 2003, Seismic Structure in the mantle beneath Australia, 7–23, in *The Evolution and Dynamics of the Australian Plate*, Ed. D. Müller & R. Hillis. Geological Society of Australia Special Publication **22** and Geological Society of America Special Paper **372**.

Kennett, B.L.N., Fishwick, S., Reading, A.M. & Rawlinson, N., 2004. Contrasts in mantle structure beneath Australia – relation to Tasman Lines?, *Austral. J. Earth Sci.*, **51**, 563–569.

Kennett, B.L.N. & Abdulah, A., 2011. Seismic wave attenuation beneath the Australasian region, *Austral. J. Earth. Sci.*, **58**, 285–295.

Kennett, B.L.N., & Furumura, T., 2008. Stochastic waveguide in the lithosphere: Indonesian subduction zone to Australian Craton, *Geophys. J. Int.*, **172**, 363–382.

Kennett, B.L.N. & Salmon, M., 2012. AuSREM: The Australian Seismological Reference Model, *Austral. J. Earth. Sci.*, in press.

Kennett, B.L.N., Salmon, M., Saygin, E. & AusMoho Working Group, 2011. AusMoho: the variation of Moho depth in Australia, *Geophys. J. Int.*, **187**, 946–958.

Khan, A., Zunino, A., Deschamps, F., 2011b. The thermo-chemical and physical structure beneath the North American continent from Bayesian inversion of surface-wave phase velocities. *J. Geophys. Res.*, **116**, B09304, doi:10.1029/2011JB008380.

Molinari, I. & Morelli, A., 2011. EPcrust : a reference crustal model for the European plate, *Geophys. J. Int.*, **185**, 352-364.

Rawlinson, N., Tkalčić, H. & Reading, A.M., 2010. Structure of the Tasmanian lithosphere from 3D seismic tomography, *Austral. J. Earth Sci.*, **57**, 381–394.

Rawlinson, N., Kennett, B.L.N., Vanacore, E., Glen, R.A., & Fishwick, S., 2011. The structure of the upper mantle beneath the Delamerian and Lachlan orogens from simultaneous inversion of multiple teleseismic datasets, *Gondwana Res.*, **20**, doi:10.1016/j.gr.2010.11.001.

Ritsema, J., Deuss, A., van Heijst, H.J. & Woodhouse, J.H., 2011. S40RTS: a degree-40 shear-velocity model for the mantle from new Rayleigh wave dispersion, teleseismic traveltime and normal-mode splitting function measurements, *Geophys. J. Int.*, **184**, 1223-1236.

Roth, E.G., Wiens, D.A., Dorman, L.M., Hildebrand, J & Webb S.C. 1999 Seismic attenuation tomography of the Tonga-Fiji region using phase pair methods, *J. Geophys. Res.*, **104**, 4795–4809

Salmon, M., Kennett, B.L.N. & Saygin, E., 2012. Australian Seismological Reference Model (AuSREM): crustal component, *Geophys. J. Int.*, in press .

Sambridge, M.S., 1999. Geophysical inversion with a neighbourhood algorithm – I. Searching a parameter space, *Geophys. J. Int.*, **138**, 479–494.

Schivardi, R. & Morelli, A., 2010. EPmantle: a three-dimensional transversely isotropic model of the upper mantle under the European Plate., *Geophys. J. Int.*, **185**, 469-484.

van der Hilst, R., Kennett, B.L.N., Christie, D., & Grant, J., 1994. Project SKIPPY explores the lithosphere and mantle beneath Australia, *EOS Trans. AGU*, **75**, 177.

Yoshizawa, K. & Kennett, B.L.N., 2002. Non-linear waveform inversion for surface waves with a neighbourhood algorithm – application to multimode dispersion measurements, *Geophys. J. Int.*, **149**, 118–133.

Yoshizawa, K. & Kennett, B.L.N., 2004. Multi-mode surface wave tomography for the Australian region using a 3-stage approach incorporating finite frequency effects, *J. Geophys. Res.*, **109**, B02310; doi: 10.129/2002JB002254.

Yoshizawa, K. & Ekström, G., 2010. Automated multimode phase speed measurements for high-resolution regional-scale tomography: application to North America, *Geophys. J. Int.*, **183**, 1538–1558.

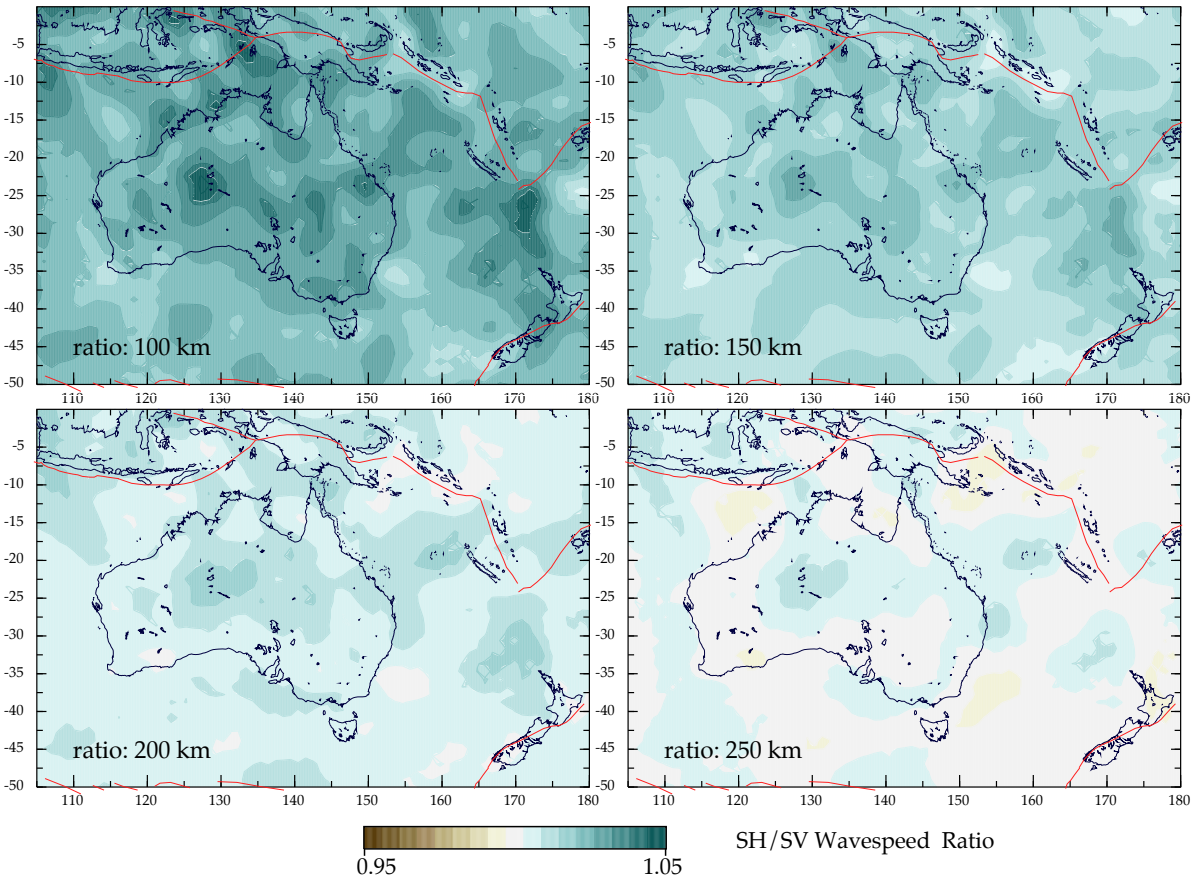

Figure A1. Slices through the smoothed SH/SV wavespeed ratio in the mantle at: 100 km, 150 km, 200 km and 250 km depth.

APPENDIX A: ALTERNATIVE CONSTRUCTION OF SH MODEL

For the SH wavespeed model shown in Figure 8 we employed information from the two recent SH models. As noted above, this lead to a rather patchy distribution of the SH/SV wavespeed ratio. For a representative model we would prefer that all components of the model are at a comparable level of smoothness, which is why we have used the SV model in the construction of the P wavespeed, density and Q^{-1} models.

We can take a comparable approach for SH by utilising a smooth SH/SV wavespeed distribution taken from the study with the broader geographic path coverage (Yoshizawa, personal communication). The pattern of the wavespeed ratio is illustrated in Figure A1, and the SH wavespeed model constructed using this ratio applied to the AUSREM SV model is shown in Figure A2. Comparison of Figure 8 and Figure A2 indicates that we have captured much of the character of the original SH model, but with slightly less heterogeneity at depth.

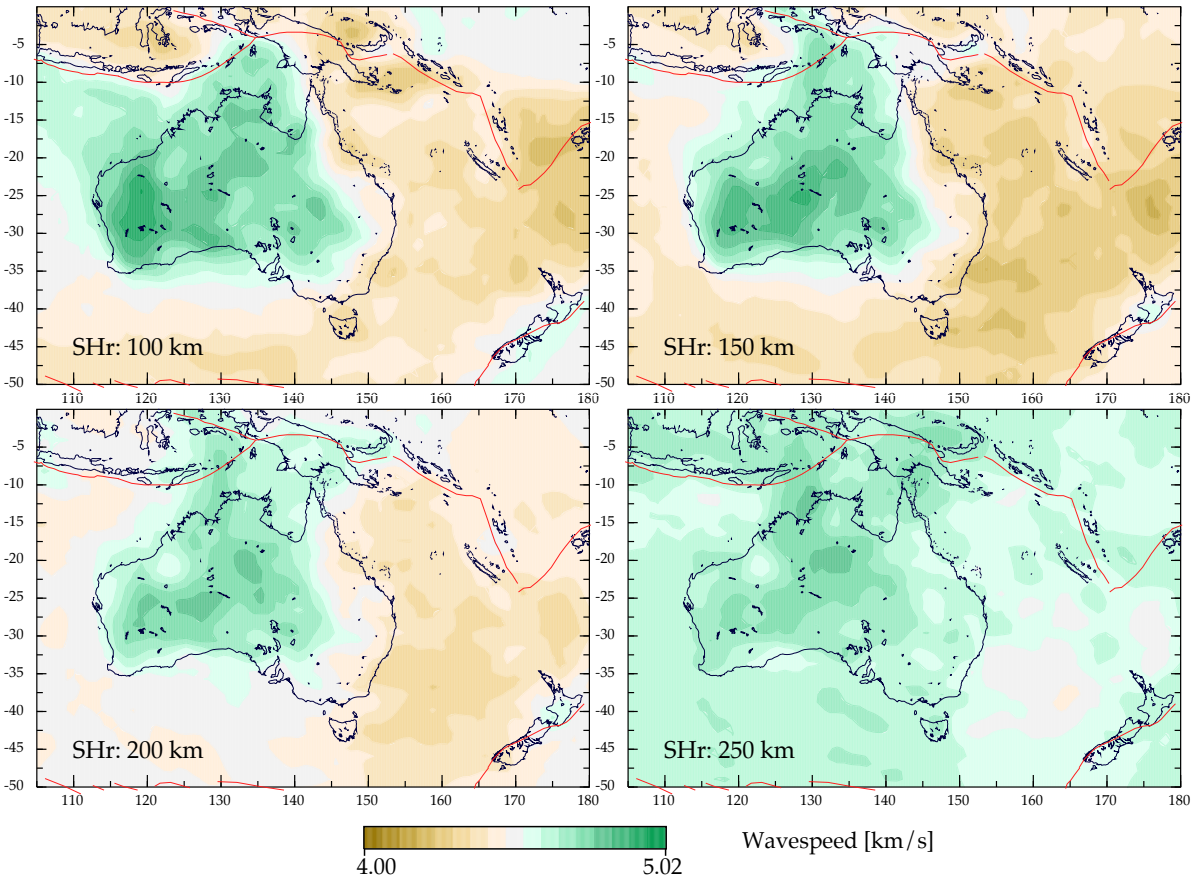

Figure A2. Slices through the alternative AuSREM mantle model for SH wavespeed, constructed from the SV model (Figure 7) with the application of the SH/SV ratio from Figure A1, at: 100 km, 150 km, 200 km and 250 km depth.

Supplementary Material:
Australian Seismological Reference Model (AuSREM):
Mantle Component

B.L.N. Kennett, A. Fichtner, S. Fishwick & K. Yoshizawa

1 COVERAGE OF TOMOGRAPHIC MODELS FROM WAVEFORM INVERSION

The AuSREM mantle model is built from a linear combination of three recent models derived by waveform fitting, using different computational procedures and data. The path coverage for each model is illustrated in Figure S-1, for the paths that are most sensitive to the fundamental mode of the Rayleigh wave. This choice indicates the maximal coverage for each of the models.

The first model is taken from Fishwick & Rawlinson (2012), in which path specific 1-D models are constructed using inversion for the fundamental Rayleigh mode and first few higher modes via the secondary variable approach of Cara & Lévêque (1987). The 1-D models are regarded as path averages through a 3-D volume and are combined in a linear inversion with regularisation to produce a 3-D model defined at 25 km intervals. This approach shows a strong influence from the fundamental Rayleigh mode and so sensitivity tends to diminish at depths below 250 km. The model exploits data from permanent and portable stations across both the Australian continent and the surrounding regions, resulting in over 13,000 paths included within the tomographic inversion.

The second model is based on a 3-stage approach (Yoshizawa & Kennett 2004) via the intermediary of multi-mode surface wave dispersion maps at many frequencies, with allowance for radial anisotropy. A fully nonlinear waveform inversion is undertaken using the Neighbourhood Algorithm (Sambridge 1999). Path-specific models from the nonlinear inversion are then interpreted as summaries of multi-mode dispersion. The reliability of estimated dispersion is evaluated by the relative modal strength and waveform fit in a time-frequency domain. A cluster analysis is then employed for eliminating outlying measurements (Yoshizawa & Ekström 2010), and eventually over 8000 paths for the fundamental mode and about 2000 paths for the higher modes are collected. For each mode a set of phase-speed maps are constructed as a function of frequency, incorporating possible off-great circle propagation and the influence zone around the propagation path which varies with frequency. Local dispersion curves are extracted and an inversion is made for a local 1-D model. Finally a 3-D model is assembled from the ensemble of local models. In this approach finite-frequency effects are included explicitly.

The third model is taken from the work of Fichtner et al. (2010) where inversion for a radially anisotropic model is made using a nonlinear inversion. The inversion is iterative with sequential linearised steps with 3-D waveform modelling at each stage, constructed using the spectral element method and an adjoint construction for the necessary derivatives for the frequency-time domain waveform fit criterion. The smooth 3-D starting model was based on the work of Fishwick et al. (2005) for wavespeeds and used the attenuation model presented in Kennett & Abdulah (2011). This is the most computationally demanding approach and in consequence the number of paths is much small (less than 1000), and azimuthal control is limited to the west of the continent. At each stage the calculations are carried out in 3-D, and full allowance is made for the spatial variation of the influence of different frequencies

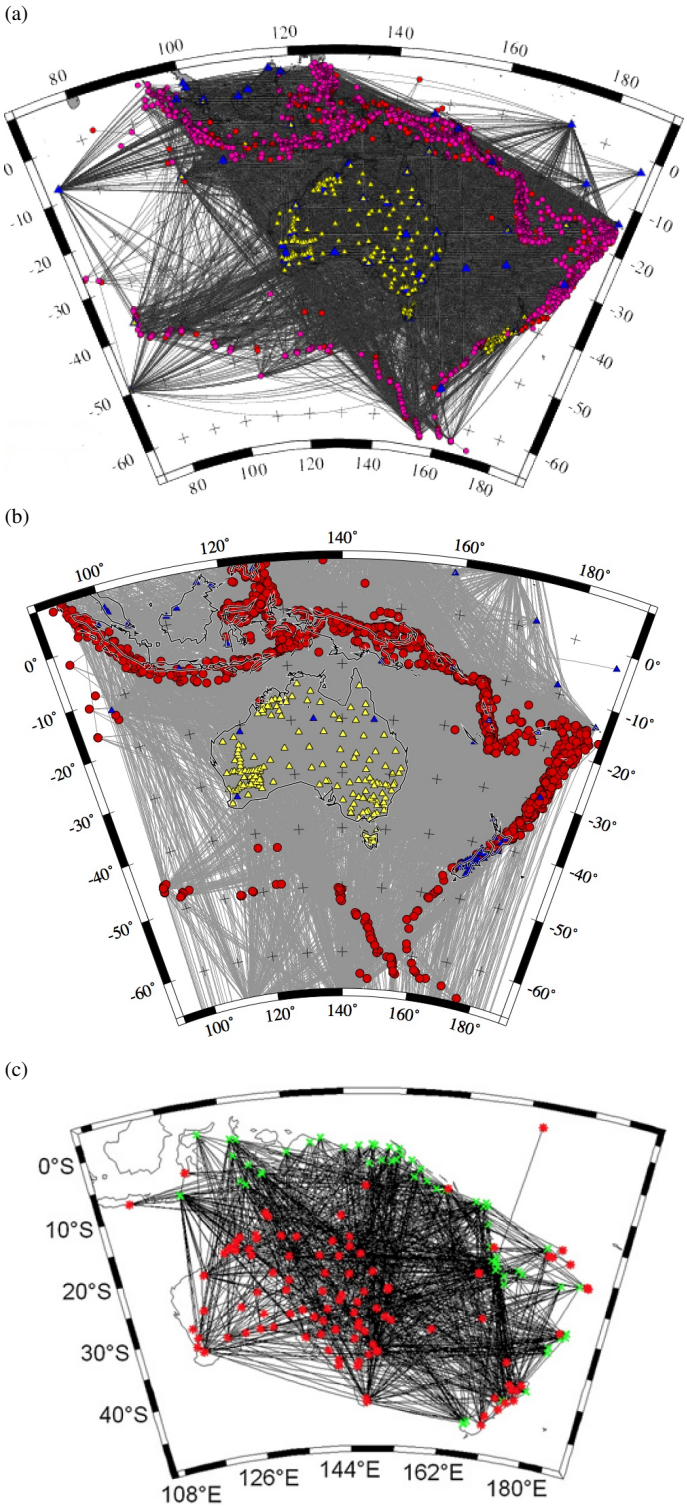

Figure S-1. Maps illustrating the path coverage of the three models used as a basis for constructing the AuSREM mantle model (a) from Fishwick & Rawlinson (2012), (b) from updated version of Yoshizawa & Kennett (2004) model, (c) from Fichtner et al (2010). In each case the coverage corresponding to the fundamental mode of Rayleigh waves is displayed.

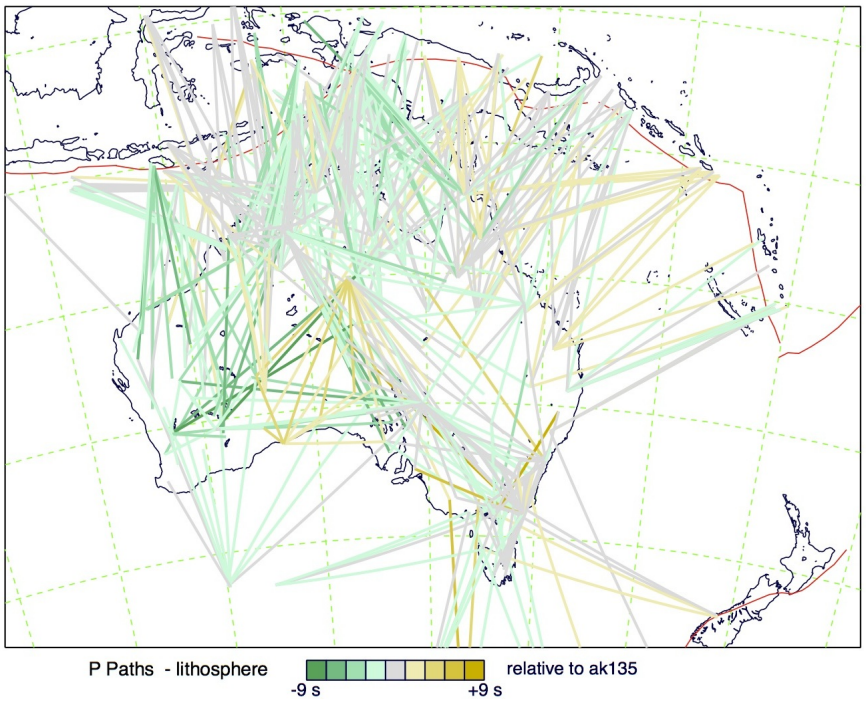

Figure S-2. P wave travel times to 18° epicentral distance from well-constrained events in and around the Australian continent shown by colour coded paths (updated from Kaiho & Kennett, 2000).

2 CONSTRAINTS FROM BODY-WAVE TRAVEL TIMES

As part of the study of refracted waves through the upper mantle undertaken by Kaiho & Kennett (2000), travel time picks were made at available stations for the best characterised regional seismic sources. This data set has subsequently been augmented using events recorded at later portable station deployments, and other information. Events out to 18° largely sample passage through the lithosphere, and provide useful direct constraints on wavespeed.

In Figures S-2, S-3 we display the travel time residuals for both P and S waves out to 18° epicentral distance, mapped onto the propagation paths from source to receiver. The coverage for P waves is better than for S because we have been able to exploit the collection of P travel times for "ground truth" events, with epicentral errors less than 5 km, made by Geoscience Australia.

Both Figures S-2 and S-3 show clear evidence for a reduction in seismic wavespeeds in the uppermost mantle beneath Central Australia confirming the results displayed in Figure 14 for SV wavespeeds at 75 km. As can be seen in Figure S-2 slightly longer P-wave paths in central Australia are much faster as they encounter the almost continuous higher wavespeeds below 100 km depth (see Figures 9, 14).

The body wave picks weew made on unflitered seismograms and emphasise the behaviour at 1 Hz and above for P waves and 0.5 Hz and above for S waves. The configuration of the regional events around Australia (see also Figure S-1) provides the unusual circumstance of having multiple independent datasets that provide control on lithospheric structure.

Abdulah (207) made travel time picks and attenuation measurements for over 4000 paths for events out to 40° epicentral distance to stations on the Austrlain Continent. There is close correspondence between his results for shorter distances and those shown in Figures S-2, S-3, though the quality of event information was more variable. A clear feature of all these studies is the distinct separation between faster wavespeeds in the centre and west of the continent and slower velocities to the east, but with notable substructure in the variations between nearby paths.

REFERENCES

Abdulah, A., 2007. *Seismic Body Wave Attenuation Tomography beneath the Australasian region*, Ph.D. Thesis, Australian National University.

Fichtner, A., Kennett, B.L.N., Igel, H. & Bunge, H.-P., 2010. Full seismic waveform tomography for radially anisotropic structure: New insights into the past and present states of the Australasian upper mantle, *Earth Planet. Sci. Lett.*, **290**, 270–280.

Fishwick S. & Rawlinson N., 2012. 3-D structure of the Australian lithosphere from evolving seismic datasets, *Aust. J. Earth Sci.*, **59**, 1-18.

Kaiho, Y. & Kennett, B.L.N., 2000. Three-dimensional seismic structure beneath the Australasian region from refracted wave observations, *Geophys. J. Int.*, **142**, 651–668.

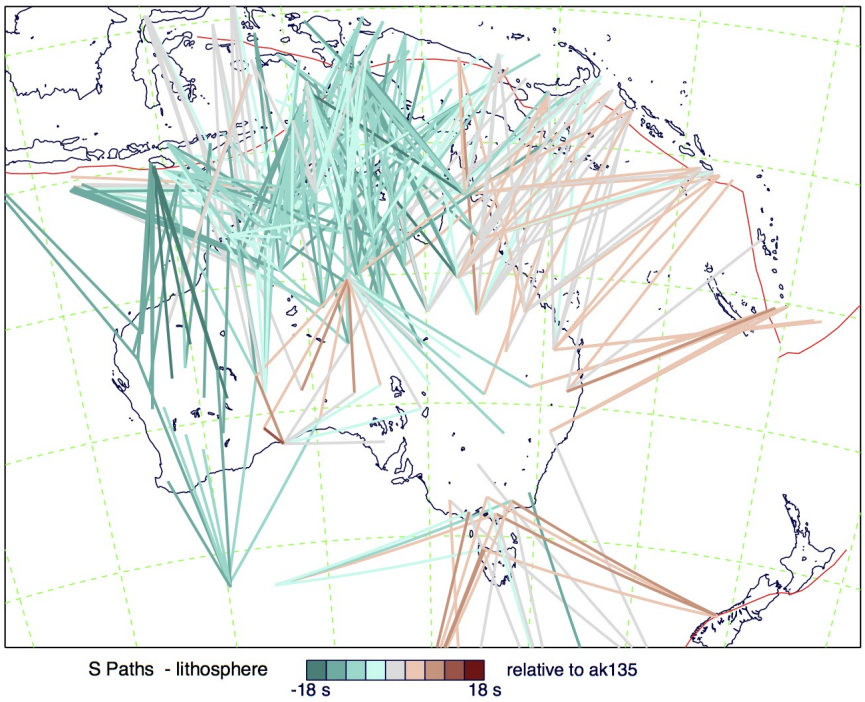

Figure S-3. S wave travel times to 18° epicentral distance from well-constrained events in and around the Australian continent shown by colour coded paths (updated from Kaiho & Kennett, 2000).

Yoshizawa, K. & Kennett, B.L.N., 2004. Multi-mode surface wave tomography for the Australian region using a 3-stage approach incorporating finite frequency effects, *J. Geophys. Res.*, **109**, B02310; doi: 10.129/2002JB002254.